Title
Mechanisms of RNA export in Caenorhabditis elegans

Author
Mellman, Katharine Sara

Publication Date
2020

Peer reviewed|Thesis/dissertation

Mechanisms of RNA export in Caenorhabditis elegans

by
Katharine Mellman

DISSERTATION
Submitted in partial satisfaction of the requirements for degree of
DOCTOR OF PHILOSOPHY

in

Cell Biology

in the

GRADUATE DIVISION
of the
UNIVERSITY OF CALIFORNIA, SAN FRANCISCO

Approved:

DocuSigned by:
Noelle L'Etoile
54CC7336DCB447E...

Noelle L'Etoile
Chair

DocuSigned by:
Kaveh Ashrafi

Kaveh Ashrafi

DocuSigned by:
Torsten Wittmann

Torsten Wittmann

DocuSigned by:
K. Mark Ansel
BC645044B450408...

K. Mark Ansel

Committee Members

Acknowledgements

I would first like to thank Noelle, for her boundless enthusiasm and drive to think outside the box. You gifted a special and invaluable perspective, completely redefining my idea of scientific inquiry. I'd also like to thank my tireless lab friends. Bo, who put up with my nonsense and kept me grounded. Sarah W, who always broadened my perspectives and countered all my luddite tendencies. Aarati who bestowed great advice and dogs. Thanks to Kelli, for welcoming me into the world of worms. Sarah N, I thank you for your companionship and I'm sorry about the owls. To Kirby, seeing you grow as a scientist is one of the most inspiring things I've experienced. Dear Mary, thanks for continuing to help me even though you've changed hemispheres. And Nando, for tolerating me and my Queen phases. Ray, you know what you've done. Matt, thanks for not killing me. And thanks to Tiffany and Veronica, without you there'd be no science.

To my committee and other advisors- Mark, Kaveh, Aimee, Maria and Torsten. Thank you for sticking it out. Thank you for your time and brains.

Stephanie and Kim, my first UCSF scientific advisors and friends. I love you both and thank you for being (to Stefan and Ken, and the wee boys too).

Jen, for keeping things in perspective.

Sasha, thanks for the long-distance encouragement and for Mila.

Peter and Sandra and Sebastian and Claudia- thanks for being supportive and keeping my well-earned mockery to a minimum.

Margy and Ira, I wouldn't have been able to do this without you. Any of it all. Thank you.

Desiree and Josh and Lauren, you saw me through the entire experience, and haven't run away yet. Thanks for being my support system, travel buddies, and partaking in my terrible ideas.

Love to my grandparents, Jack who was here for part of it, Joan who still is, and Marty and Sara who could only imagine it.

Love to you all.

Mechanisms of RNA export in *Caenorhabditis elegans*

Katharine Sara Mellman

Abstract

Many mechanisms govern both how animals respond to stimuli and how these responses inform physical state and future behavior. In *Caenorhabditis elegans*, these mechanisms include the generation and spread of various species of small RNAs. Emerging as a potent regulator of gene expression in both a single animal and its progeny, small RNAs are reshaping the fields of behavior and transgenerational inheritance. The rising prominence of small RNA within the context of these fields highlights gaps in the knowledge of essential processes, such as the precise mechanisms of small RNA export. RNA import, thanks to earlier efforts characterizing systemic RNA interference (RNAi), are relatively well understood. However, much less is known about how RNAi and other small RNA exit cells. This manuscript details tools and approaches for identifying mobile small RNAs, members of RNA export pathways, and points of regulation in the export process.

Table of Contents

List of Figures

List of Tables

Introduction

Life has evolved in the presence of competing and varying external pressures. In an ecosystem, organisms thrive when they are able to sense cues associated with these pressures and navigate the shifting circumstances. These pressures can range from temperature to food availability and the detection of associated cues is only one part of the survival equation. These cues must be interpreted, weighed against each other, and appropriately responded to.

There exists vast diversity in how organisms accomplish these goals. In the case of the free-living nematode, *Caenorhabditis elegans*, sensory neurons detect changes in the immediate environment. These neurons can then in turn communicate with other neurons and somatic tissues via canonical neural signaling. However, this is not the only mechanism by which sensory neurons signal other cells. Detecting a cue initiates a variety of events within a sensory neuron. The following manuscript explores one facet of this response, the modification of the intracellular RNA landscape, and the mechanisms by which this changing landscape can manifest itself in the body of a worm.

Chapter 1

Abundance of endogenous small RNAs in different behavioral states

Bacteria growing on decaying vegetal matter serve as a primary food source for *C. elegans*. These sources emit an array of volatile odors, which enable the animals to locate them (Shulenburg & Felix, 2017). However, because these odors are not limited to nutritious bacteria, the worm needs an additional mechanism to assess the value of food sources. The odor butanone ($5x10^{-3}$ dilution) is an innately attractive volatile odor detected by the AWC sensory neuron (C. I. Bargmann, Hartwieg, & Horvitz, 1993). However, this and other attractive odors lose their appeal when a worm is starved for 80 minutes in the presence of the odor, a process called adaptation (Heather A. Colbert & Bargmann, 1995) (H A Colbert & Bargmann, 1997). Further complicating the value of this innately attractive odor, butanone is emitted by pathogenic bacteria, such as *Serratia marcescens* (Worthy et al., 2018). A worm cannot rely upon a single cue. By integrating various signals, the worm is able to determine if butanone is a reliable signal of food, thereby increasing its overall fitness.

In a laboratory setting, a worm's preference for an odor is measured by a chemotaxis assay. Following a period of starvation and in the presence of odor or buffer alone, populations of animals are placed on a chemotaxis plate. The plate presents two options to the worm, an odor spot (in this case butanone) and a negative control spot. These spots also contain the paralytic agent sodium azide (NaN_3), allowing the number of animals to be counted after a 2 hour "roaming" period. The number of animals at the control spot is subtracted from the number of animals at the odor spot, and this value is divided by the total number of animals on the plate. An index approaching 1 indicates the animals are attracted to the odor. An index close to 0 indicates the animals have lost their preference or are repulsed by the odor spot (Figure 1.1).

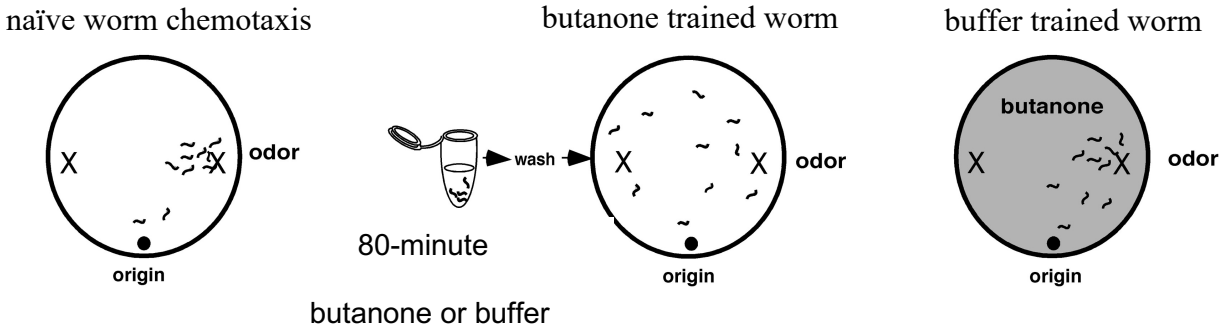

Chemotaxis Index (CI) = $\frac{\text{(\# animals at odor spot) – (\# animals at control spot)}}{\text{total number of animals plated}}$

Figure 1.1
Butanone training and chemotaxis assay
After 2 hours roaming time, well-fed, untrained worms will populate the odor spot, resulting in a chemotaxis index approaching 1. Starved, butanone trained worms show no preference or repulsion from odor spot, resulting in a chemotaxis index around 0. Starved, buffer trained worms maintain attraction towards butanone and have a chemotaxis index approaching 1. Adapted from (L'Etoile et al., 2002).

Behavioral adaptation is promoted by a series of intracellular events in the AWC neuron. In a starved worm, prolonged odor stimulation causes the cGMP dependent protein kinase EGL-4 to enter the nucleus (L'Etoile et al., 2002). Here, it in engages in nuclear RNAi to silence *odr-1*, a putative guanylyl cyclase expressed in the butanone-detecting sensory neuron AWC and required for normal responses to odors detected by this neuron, particularly butanone (Juang et al., 2013). With decreased *odr-1* transcription, it is likely that less receptor occupies the cell membrane and butanone loses its appeal (Figure 1.2).

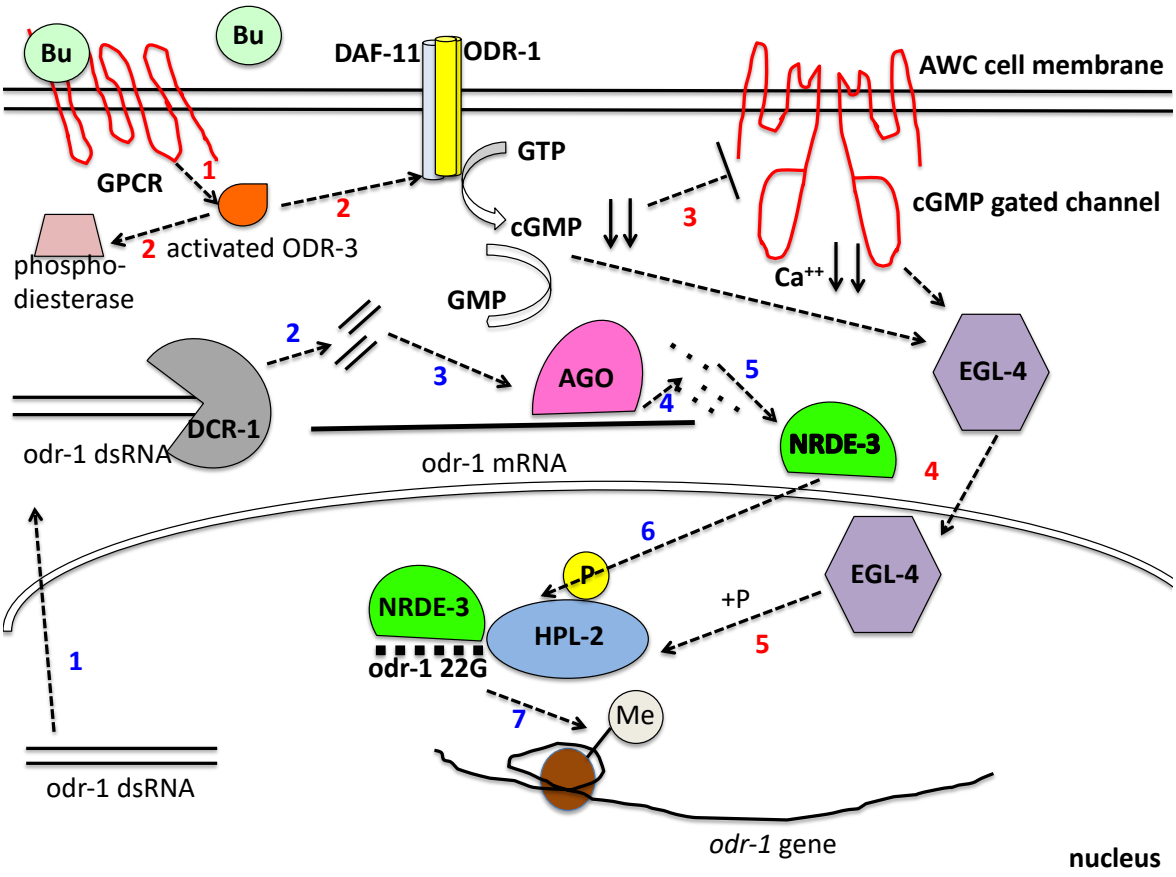

Figure 1.2
22G RNA biosynthesis in the context of butanone adaptation
Odor Adaption Pathway (in red): Odor sensing GPCRs activate G-aplha ODR-3 (1). ODR-3 stimulates the production cGMP which gets converted into GMP (2). Intracellular levels of cGMP fall, inactivating cGMP gated channels causing intracellular Ca++ levels to fall (3). The combination of reduced cGMP and Ca++ cause EGL-4 to enter the nucleus, thereby initiating long term adaptation (4). EGL-4 phosphorylates HPL-2 (5).
22G RNA Biosynthesis pathway (in blue): *odr-1* dsRNA is exported to the cytoplasm (1). Here, it associates with DCR-1 to form 26nt primary siRNA (2). These 26 nt primary siRNAs are loaded onto an argonaute where they facilitate post-transcriptional gene silencing in the cytoplasm and generate 22G RNAs (4). 22G RNAs are loaded onto NRDE (5). This complex is translocated back into the nucleus, where it associates with phosphorylated HPL-2 (6). This complex then deposits H3K9 methylation marks to silence odr-1 transcription (7). (Castel & Martienssen, 2013) (Juang et al., 2013) (Cornelia I. Bargmann, 2006)

During the process of butanone adaptation induced nuclear RNAi, 22G RNAs are produced from the *odr-1* gene. 22G RNAs are RNA dependent RNA polymerase (RdRDP) derived small RNAs that possess a 5' Guanosine residue and are 22 nucleotides in length (Gu et al., 2009). They act through argonautes (AGOs) to target a specific gene for transcriptional silencing via H3K9 methylation (Figure 1.2).

Published data indicate the abundance of one such 22G RNA, odr-1.7, rises in both the AWC neuron and entire body during adaptation (Juang et al., 2013). By nature of the silencing mechanism, 22G RNA abundance increases as the target mRNA is degraded. As this silencing signal moves beyond its cell of origin, it likely propagates itself in target tissues. Additional evidence demonstrates HRDE-1, a germline specific AGO, binds odr-1.7 (Buckley et al., 2012). These studies, taken together, hint at an interesting biological phenomenon as well as a potential mechanism by which environmental cues can impact gene expression in future generations. It is known that DNA methylation is a mechanism of epigenetic inheritance (Dias & Ressler, 2014). However, the manner in which these marks are targeted to specific genes remains unclear. The transmission of 22G RNA species may offer an analogous explanation to fill this gap and further elucidate this mode of inheritance.

odr-1 22G RNA abundance

Previous work in the L'Etoile lab explored the relative abundance of one species of 22G RNA, odr-1.7, in various behavioral states and genetic backgrounds (Juang et al., 2013). qPCR data show that upon adaptation, odr-1.7 22G RNA increased compared with unc-40 22G RNA control in wild-type animals (Figure 1.3). This is consistent with the decrease in *odr-1* mRNA in adapted worms (Figure 1.4). In mutant animals deficient in either a dsRNA import channel (*sid-*

1) or 22G RNA biosynthesis pathway (*mut-7*), there was no increase in odr-1.7 compared to control (Figure 1.3). This increase was partially restored in transgenic animals expressing an AWC specific MUT-7, a limited rescue of the 22G biosynthetic pathway (Figure 1.3). In these mutant and transgenic animals, mRNA abundance negatively correlated with odr-1.7 22G abundance in cognate populations (Figure 1.4). (Juang et al., 2013).

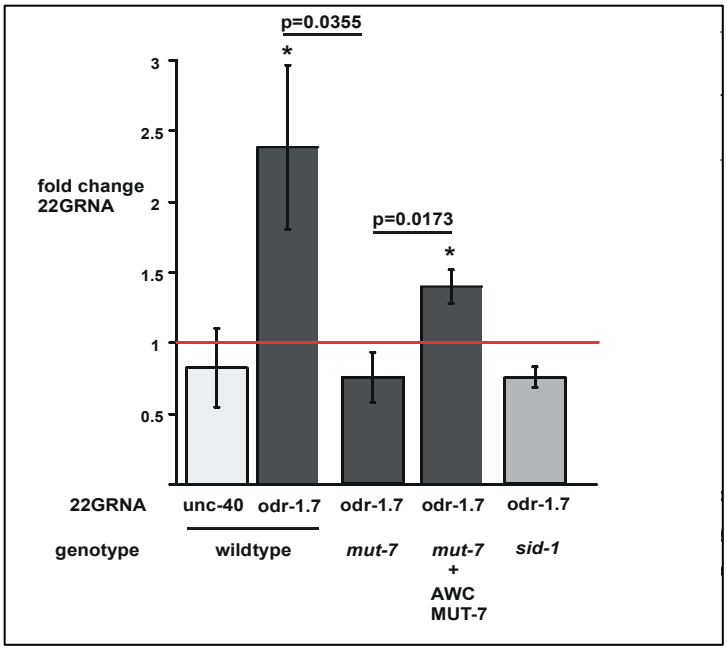

Figure 1.3
22G RNA fold changes in butanone adapted worms of varying genetic backgrounds.
22G RNA abundance fold change in butanone adapted worm populations vs buffer trained worm populations. unc-40.2 22G serves as a control, with no change between butanone adapted and buffer trained populations. odr-1.7 increases in butanone adapted populations in a wild-type background. odr-1.7 fails to increase in populations deficient in the 22G biosynthesis pathway (*mut-7*) and RNA import (*sid-1*). Reconstituting the 22G biosynthetic pathway in AWC neurons (under *ceh-36* promoter) partially rescues odr-1.7 increase in butanone adapted populations. *mut-7* experiments taken from Juang et al., 2013. Fold changes of 22G RNAs in wild-type, *mut-7, mut-7* + pceh-36:MUT-7, and *sid-1* animals.

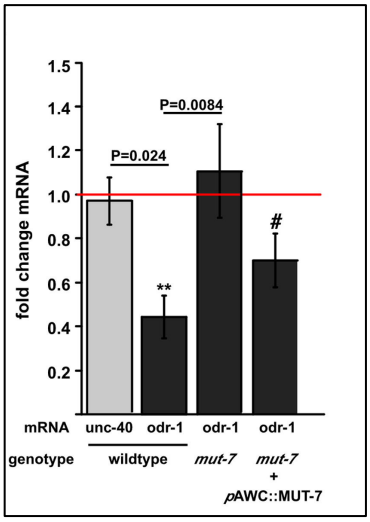

Figure 1.4
mRNA fold changes in butanone adapted worms of varying genetic backgrounds
mRNA abundance fold change in butanone adapted worm populations vs buffer trained worm populations. *unc-40* mRNA serves as a control, with no change between butanone adapted and buffer trained populations. *odr-1* mRNA decreases in butanone adapted populations in a wild-type background. odr-1 mRNA fails to decrease in populations deficient in the 22G biosynthesis pathway (*mut-7*). Reconstituting the 22G biosynthetic pathway in AWC neurons (under *ceh-36* promoter) partially rescues *odr*-1 mRNA decrease in butanone adapted populations.
From (Juang et al., 2013).

Multiple small RNA sequencing libraries indicate that odr-1.7 is one of many species of 22G RNAs clustered at the 15th and 16th exons in the *odr-1* gene (Figure 1.5). I sought to identify additional behaviorally relevant 22G RNAs in this region to serve as a robust read out for future endogenous small RNA (endo-siRNA) experiments. To expand on the existing odr-1.7 data, I generated probes to look at abundant 22G RNAs in this "peak" area. The probe sequences were taken from three libraries: 1) a small RNA library generated in the Mello lab (Gu et al., 2009) 2) a library of small RNAs bound to a germline argonaute (HRDE-1) from the Kennedy lab (Buckley et al., 2012) and 3) a series of small RNA libraries generated in the L'Etoile lab in 2015 (unpublished). These seven probes span both the exonic and intronic region between the 15th and 16th exon of *odr-1* (Figure 1.6) (Table 1.1).

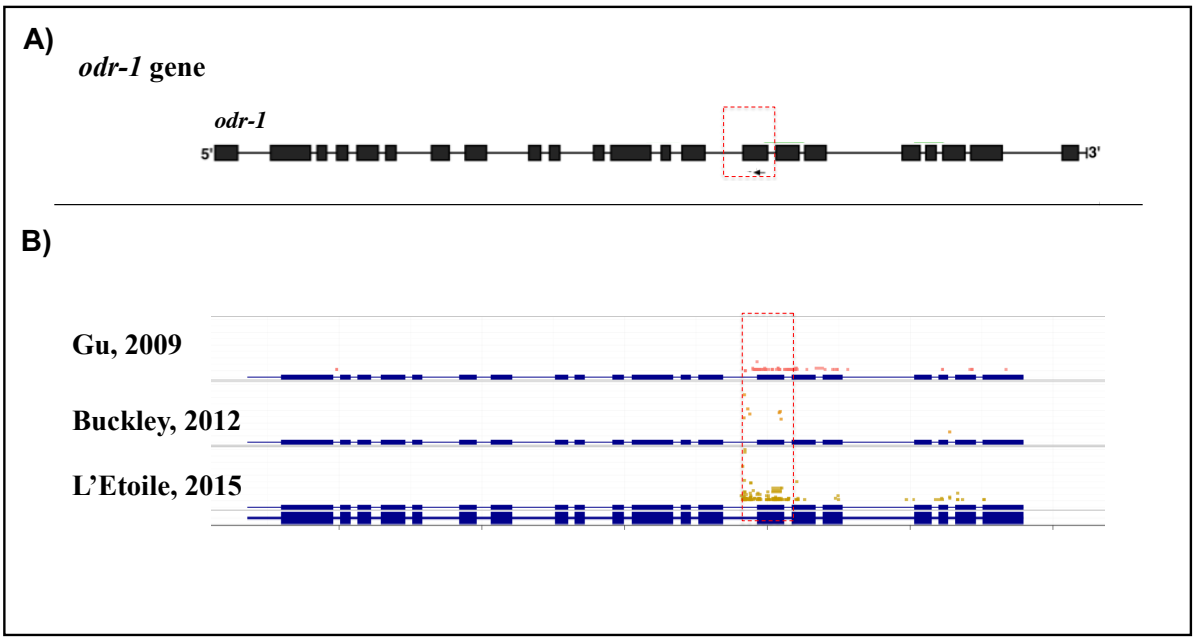

Figure 1.5
odr-1 22G RNA locations
A) Complete *odr-1* gene with location of odr-1.7 indicated in dashed red box. From (Juang et al., 2013). B) Partial *odr-1* gene with 22G RNA hits from three RNA sequencing libraries. In descending order, Gu (2009) small RNA library generated in the Mello Lab, Buckley (2012), germline specific argonaute (HRDE-1) Co-IP generated in the Kennedy Lab, L'Etoile (2015), small RNA library generated by Sarah Gerhart and Sanjeev Balakrishnan in the L'Etoile Lab.

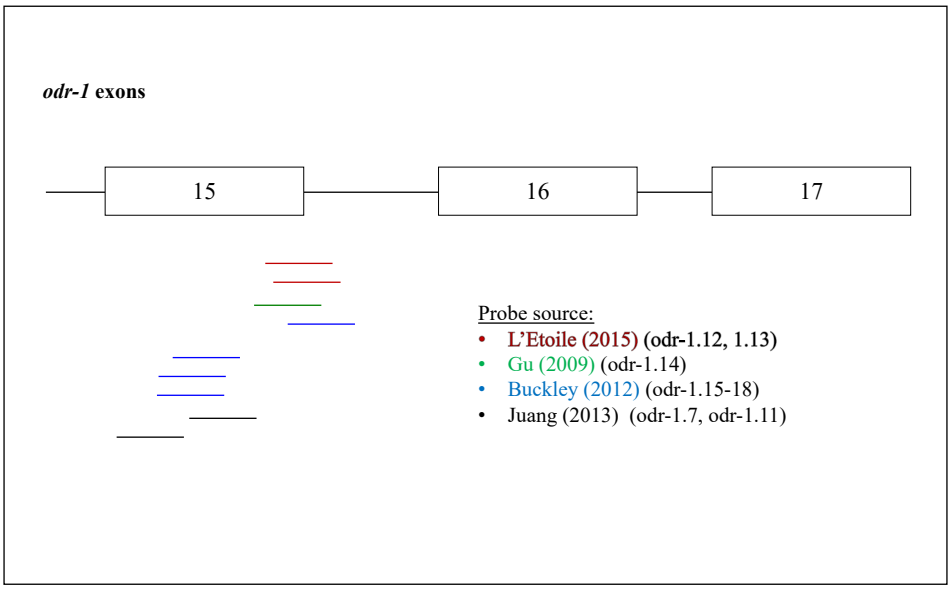

Figure 1.6
Location of 22G RNA probes
Probes generated by data from 3 small RNA libraries and one published manuscript, focusing on exons 15-17 of *odr-1* gene.

Table 1.1
odr-1 TaqMan probes
7 novel design, odr-1.7 previously published, and unc-40.2 control. Library source, sequence and location relative to exon/intron also listed.

Name	Source	Sequence	Location
odr-1.12	L'Etoile 2015	gtaagttactggaatcgagaag	exon-intron boundary
odr-1.13	L'Etoile 2015	gtaagttactggaatcgagaagt	exon-intron boundary
odr-1.14	Gu 2009	gagggtaagttactggaatcga	exon-intron boundary
odr-1.15	Buckley 2012	gttactggaatcgagaagttgg	exon-intron boundary
odr-1.16	Buckley 2012	gggaagcaaacatattgagggta	exon
odr-1.17	Buckley 2012	gaatgtgctcaggtgggaagca	exon
odr-1.18	Buckley 2012	gaatgtgctcaggtgggaagca	exon
odr-1.7	Juang 2013	gcaaacatattgagggtaagt	exon
unc-40.2	off-target control	ggatcagaatcagagcaaacgc	

Juang et al., 2013 demonstrated that the abundance of odr-1.7 rises in populations of butanone adapted animals. I repeated the same training paradigm, adhering to strict behavioral parameters. To be considered adapted, the chemotaxis index of a population must be below 0.3. To be considered properly behaving, the minimum chemotaxis index was 0.75. Small RNA was harvested from paired populations (trained/untrained) and measured using TaqMan probes. In all probes, I was unable to detect any significant fold changes in 22G RNA abundance in behaviorally adapted compared to buffer trained animals. Further, I was unable to detect any trends within individual probes across biological replicates (Figure 1.7). Closer analysis of the normalized qPCR data also failed to yield any discernable trend between the two behavioral states (Figures 1.9-12).

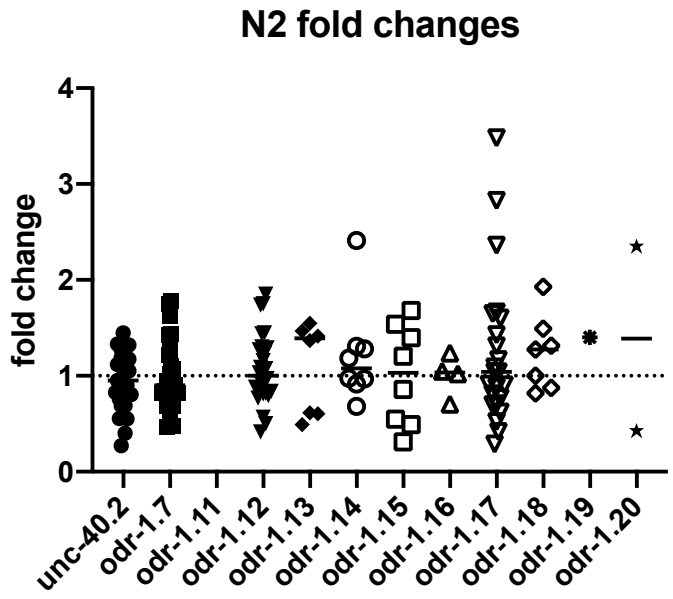

Figure 1.7
Fold changes in *odr-1* 22G RNA probes
No probe demonstrated and fold change significantly different from the control, unc-40.2 in a wild-type background. Further, no consistent pattern of fold change between butanone adapted and buffer trained animals was found within a single 22G RNA species. Fold changes ranged widely. All probes were run with unc-40.2 control. unc-40.2 control: 2-3 experimental replicates for each of 10 biological replicates. odr-1.7: 2-3 experimental replicates for each of 10 biological replicates. odr-1.11: probe failure. odr-1.12: 2-3 experimental replicates for each of 10 biological replicates. odr-1.13: 2 experimental replicates for each of 4 biological replicates. odr-1.14: 2 experimental replicates for each of 4 biological replicates. odr-1.15: 2 experimental replicates for each of 4 biological replicates. odr-1.16: 2 experimental replicates for each of 2 biological replicates. odr-1.17: 2-3 experimental replicates for each of 10 biological replicates. odr-1.18: 2 experimental replicates for each of 4 biological replicates. odr-1.19: n=1. odr-1.20: 2 biological replicates, 1 experiment each.

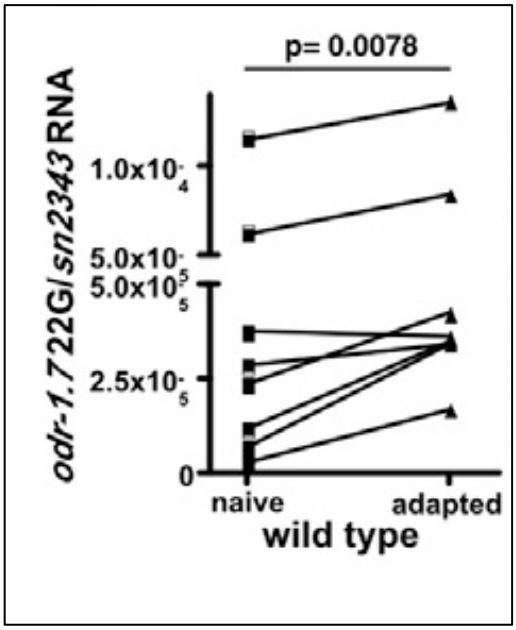

Figure 1.8
odr-1.7 abundance in butanone trained and buffer trained animals
Abundance of odr-1.7 increases in butanone trained (adapted) animals compared with buffer train animals (naïve). Paired values normalized to housekeeping small nuclear RNA sn2343. p=0.0078. Adapted from Juang et al., 2013.

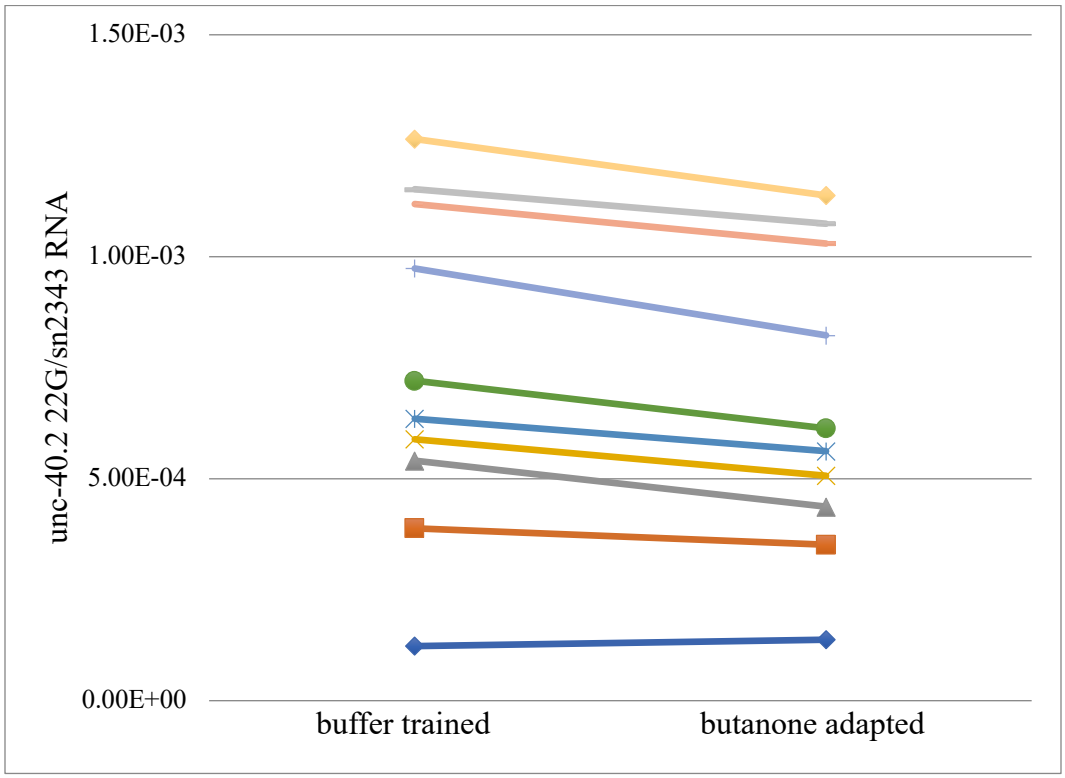

Figure 1.9
unc-40.2 abundance in butanone trained and buffer trained animals
No significant change in between buffer trained and butanone adapted animals in the control probe of 22G RNA unc-40.2. Values normalized to housekeeping small nuclear RNA sn2343. n=10 biological replicants. p=0.3757.

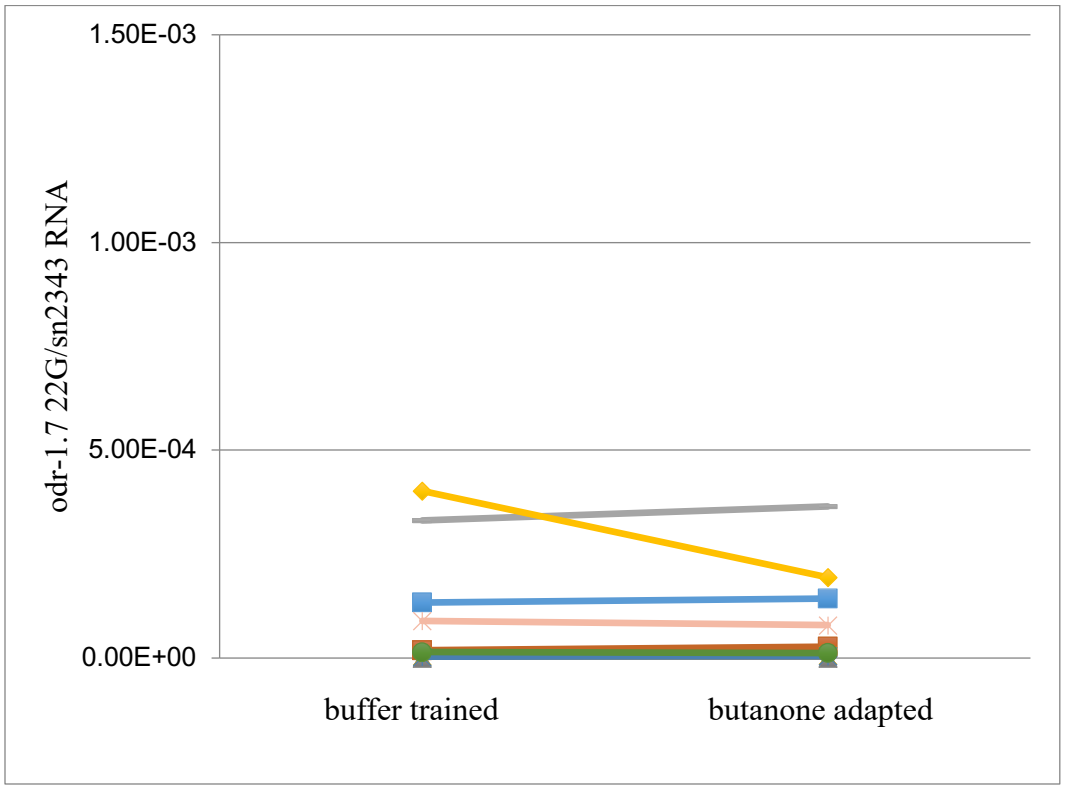

Figure 1.10
odr-1.7 abundance in butanone trained and buffer trained animals
No significant change between buffer trained and butanone adapted in probe of odr-1.7. Values normalized to housekeeping small nuclear RNA sn2343. n=5 biological replicates. p=0.6869

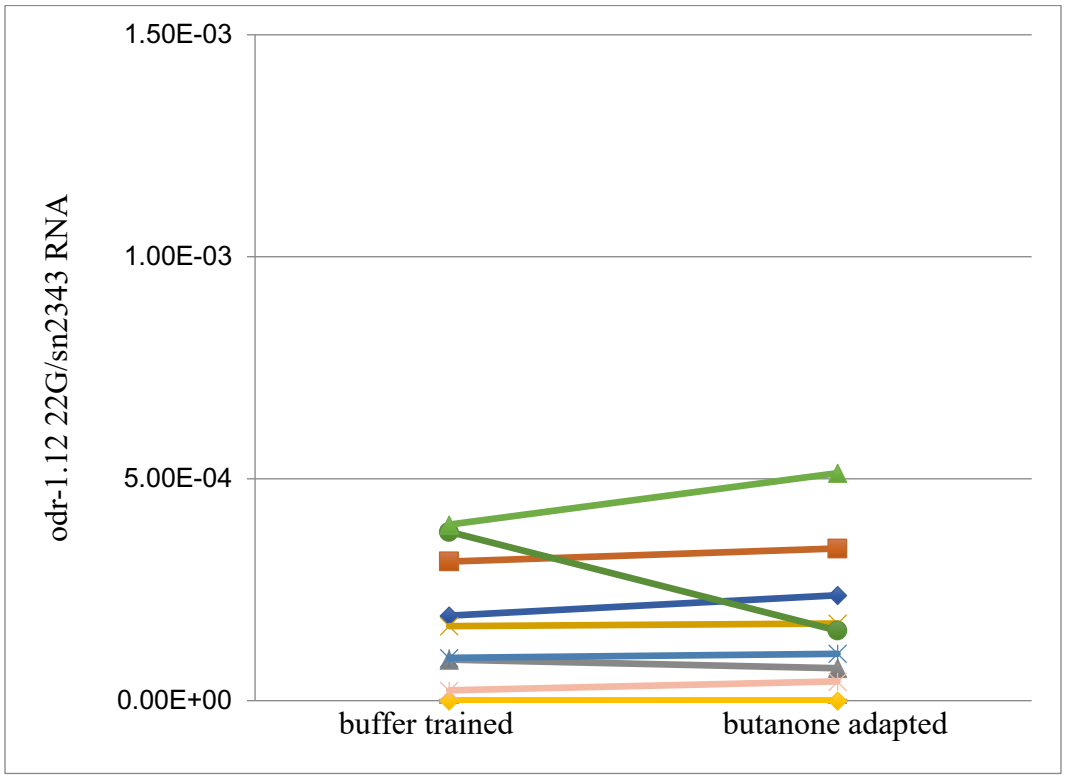

Figure 1.11
odr-1.12 abundance in butanone trained and buffer trained animals
No significant change between buffer trained and butanone adapted probe of odr-1.12. Values normalized to housekeeping small nuclear RNA sn2343. n=9 biological replicates. p=0.2975

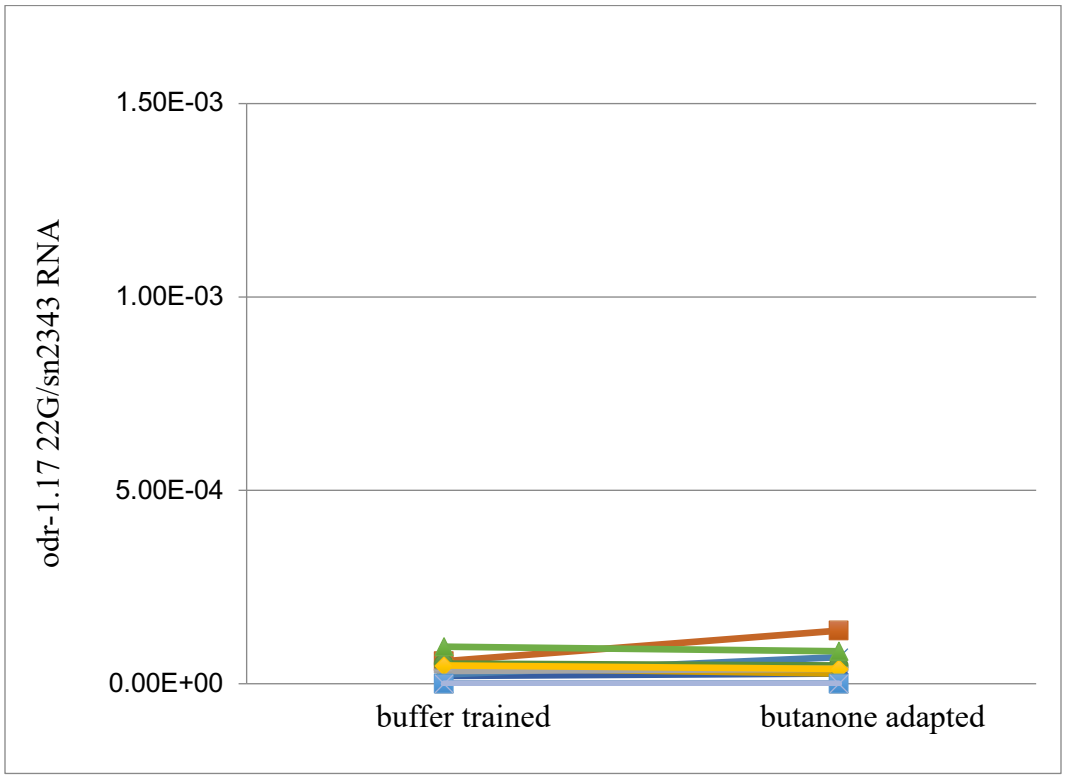

Figure 1.12
odr-1.17 abundance in butanone trained and buffer trained animals
No significant change between buffer trained and butanone adapted probe of odr-1.17. Values normalized to housekeeping small nuclear RNA sn2343. n=8 biological replicates. p=0.3288

I concurrently investigated the presumed requirement of AWC for the initiation of behaviorally mediated *odr-1* 22G RNA rise. In this effort to determine if AWC is the sole source for 22G RNA mediated silencing of *odr-1*, I probed adapted and buffer trained animals carrying a mutation (*ceh-36)* preventing AWC fate specification. Similar to the wild-type animals, I detected no change in 22G RNA abundance (unc-40.2, odr-1.7, odr-1.12, odr-1.17, odr-1.18) between adapted and buffer trained populations (Figure 1.13). AWA neurons are another class of neurons that detect innately attractive odors, but not butanone. I similarly probed an AWA fate specification mutant (*odr-7)* for changes in 22G RNA abundance but detected no fold changes in butanone adapted animals (Figure 1.14).

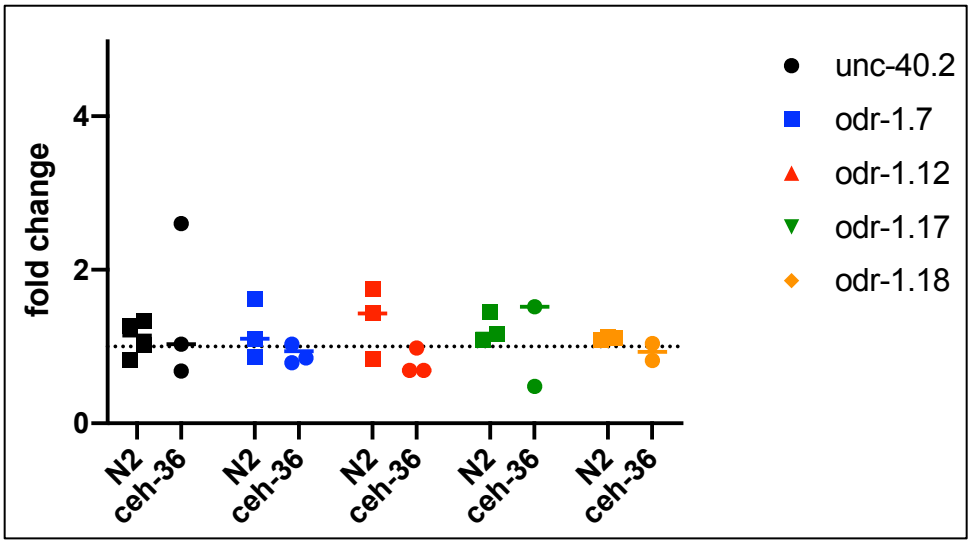

Figure 1.13
Fold changes in *odr-1* 22G RNA in wild-type vs *ceh-36* mutant animals
Fold changes between butanone adapted and buffer trained animals using 5 22G RNA probes in wild-type and AWC neuron deficient animals. No significant fold changes observed. 2 biological replicates repeated 1-2 times.

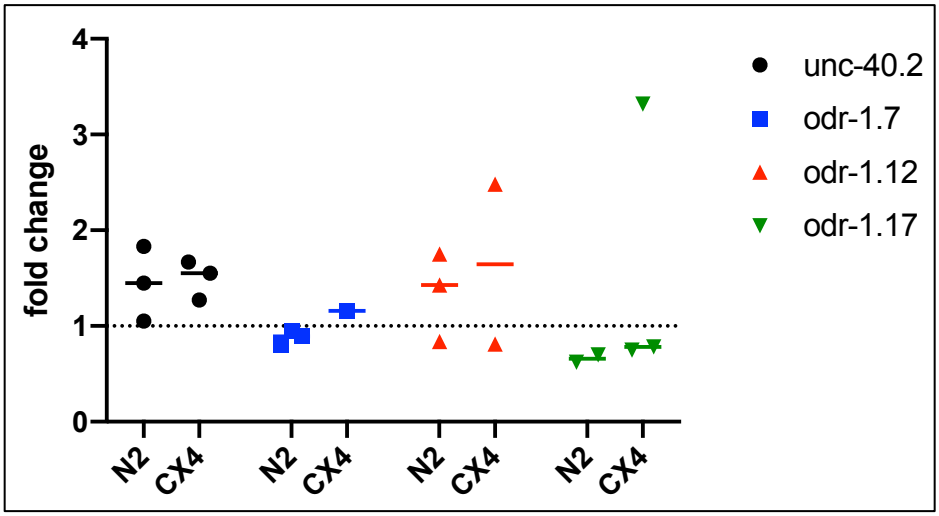

Figure 1.14
Fold changes in *odr-1* 22G RNA in wild-type vs *odr-7* mutant (CX4) animals
Fold changes between butanone adapted and buffer trained animals using 4 22G RNA probes in wild-type and AWA neuron deficient animals. No significant fold changes observed. 1-2 biological replicates repeated 1-2 times.

In these series of experiments, I have been able to demonstrate that behaviorally mediated or correlated changes in *odr-1* 22G RNA abundance is a phenomenon with many unknown parameters. The dissonance between previously published and current results may indicate a control failure on one or both series of experiments. A variety of external pressures likely affect the small RNA landscape of a worm, including past history, temperature, humidity as well as other factors. Any trends emerging from early data were silenced by additional biological replicates. Moving forward with this course of study requires an expansion of potential targets, and verification of biological relevance and reproducibility.

Mobile species of 22G RNA

The abundance of 22G RNAs is dynamic and variable in worms. By nature of their biogenesis, transmission to new tissues silences target genes while increasing their number. However, their mechanism of spread remains elusive. SID-1 is a well-defined dsRNA channel required for import of exogenous RNAi and has been partially implicated in the transport of other RNA species (William M. Winston, Christina Molodowitch, & Craig P. Hunter, 2002) (Jose, Garcia, & Hunter, 2011). Using these reports, we decided to compare small RNA libraries produced from wild-type and *sid-1*, transport defective, mutant animals. If endo-siRNAs are unable to spread to target tissues, they are unable to amplify. We compared small RNA sequencing libraries generated in the L'Etoile lab by Sarah Gerhart with analysis help from Sanjeev Balakrishnan. We focused on 22G RNAs exhibiting a fold change in excess of 2. Our targets were further culled to genes reportedly expressed in neurons only, bringing the number of candidates to 300. At this point we had a list of genes expressed in neurons with significant differential expression of 22G RNAs in *sid-1* mutant populations. To further improve the possibility that this group contained truly mobile RNAs, we selected 22G RNAs that were additionally detected in the germline via HRDE-1 Co-IP (Buckley et al., 2012) (Figure 1.15).

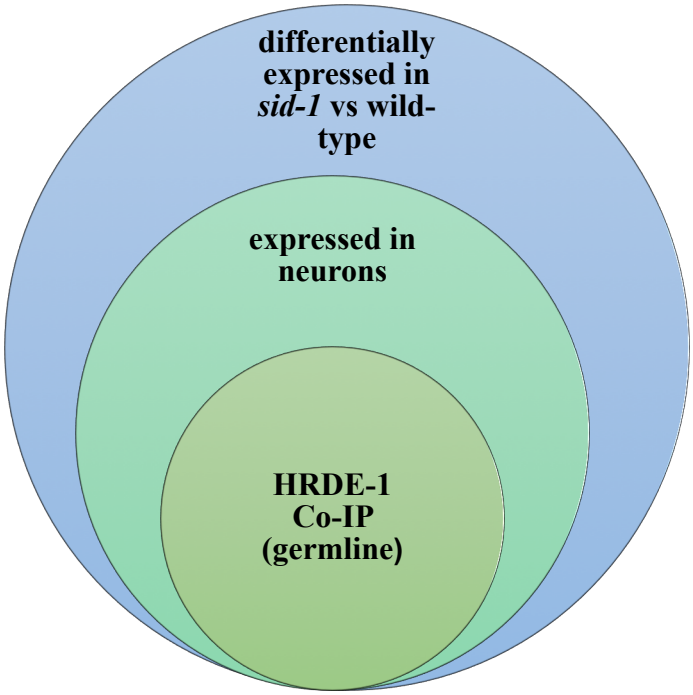

Figure 1.15
Selection of candidate genes for mobile 22G RNA
The first round of selection was based on the differential expression of 22G RNAs in small RNA libraries generated from *sid-1* mutant and wild-type populations. The second round of selection required that these differentially expressed 22G RNAs target genes that are reportedly only expressed in neurons. The third criteria requires 22G RNAs targeting candidate genes also be found in the germline, as determined by HRDE-1 Co-IP.

The top candidate meeting these criteria is *dyf-3*, a gene expressed in many chemosensory neurons and required for normal assembly of middle and distal ciliary segments (Starich et al., 1995) (Murayama et al, 2005) (Table 1.2). I generated a series of synthetic RNA oligos and TaqMan probes targeting several species of *dyf-3* 22G RNA to quantify the abundance of 22G RNAs in various genetic and environmental backgrounds (Table 1.3). The endogenous 22G RNA sequences presented structural problems with respect to oligo synthesis. Further, the TaqMan probes were unable to detect any small RNA species in multiple biological samples (Table 1.4). Despite high abundance in many small RNA sequencing libraries, I was unable to

detect individual species of *dyf-3* 22G RNA via qPCR. The sequences likely presented structural problems with respect to artificial synthesis and detection.

Table 1.2
dyf-3 meets all criteria for potentially mobile 22G RNAs
dyf-3 is expressed only in the neuron. Library comparisons demonstrate a decrease in 22G RNAs in sid-1 mutants. 22G RNA targeting *dyf-3* is found bound to HRDE-1 in the germline.

endo- siRNA	(log_2) fold change	P value (adjusted)	Base Mean	HRDE ChIP
dyf-3a	-2.15	$3.68x10^{-34}$	129.5672279	131
dyf-3b	-2.18	$6.04x10^{-22}$	54.79505166	382
dyf-3c	-2.17	$1.09x10^{-21}$	92.47688228	496
dyf-3d	-1.74	$3.71x10^{-17}$	76.0122667	109
dyf-3e	-2.01	$3.88x10^{-8}$	226.8360997	130
dyf-3f	-2.03	$9.23x10^{-6}$	12.65697315	74

Table 1.3
Sequences for *dyf-3* 22G RNA targets
Probe sequences submitted for TaqMan primer and probe design, location on *dyf-3* gene, and library source of hit.

	probe sequence	start	source
dyf-3.1	ccuaccuaggcgacaaagaagg	3397612	Gu, 2009
dyf-3.5	auaaaguuaaaggggguaggua	3397635	Gu, 2009
dyf-3.12	ccuuguuggagauuuugaucug	3398797	Buckley, 2012
dyf-3.13	aauauauuccaaaguggaccga	3398838	Buckley, 2012
dyf-3.3	gugcuuauauagaccugaugac	3398656	L'Etoile, 2015
dyf-3.15	acuuacuucuuucuuuggcacu	3398679	L'Etoile, 2015
dyf-3.18	gagacauuuauuuatgugcuua	3398641	L'Etoile, 2015

Table 1.4
C(t) values of *dyf-3* 22G RNA TaqMan qPCR
Small RNA TaqMan probes designed against *dyf-3* 22G RNA failed to detect any signal. 5 different samples were used: well fed wild-type worms (N2 0'), 30 minute starved wild-type worms (N2 30'), 60 minute starved wild-type worms (60' N2), wild-type worms exposed to pathogenic Serratia marcescens (SM) and daf-2 mutant worms (daf-2).

sample date/RNA extraction/qPCR date	N2 0' (10/26/15)/ (11/8/15)/ (11/16/15)	N2 30' (10/26/15)/ (11/8/15)/ (11/16/15)	N2 60' (10/26/15)/ (11/8/15)/ (11/16/15)	SM (11/1)/ (11/8)/ (11/17)	daf-2 (10/24)/ (11/8)/ (11/10)
sn2343 (control)	27.96	27.12	26.1	23.25	25.25
dyf-3.1	n/a	n/a	n/a	n/a	n/a
dyf-3.3	n/a	n/a	n/a	n/a	n/a
dyf-3.5	n/a	n/a	n/a	n/a	n/a
dyf-3.12	n/a	n/a	n/a	n/a	n/a
dyf-3.13	n/a	n/a	n/a	n/a	n/a
dyf-3.15	n/a	n/a	n/a	n/a	n/a
dyf-3.17	n/a	n/a	n/a	n/a	n/a

I expanded the search for mobile 22G RNAs to the next top 9 candidates (Table 1.5). While all these candidates potentially generate mobile RNAs, these mobile RNAs are not necessarily biologically relevant. To probe the biological relevance of these species, I confirmed if gene expression was modified in worm populations exposed to certain environmental challenges. If mRNA concentration correlates robustly and repeatedly with previously published data, the candidate gene may undergo 22G RNA mediated gene silencing. I first challenged these worms to a 60-minute period of starvation. mRNA extracted from multiple biological replicates failed to cluster in initial experiments. Due to this early ambiguity, this line of inquiry was not pursued further (Figure 1.16). I also subjected worm populations to *Serratia marcescens* contamination. Animals were exposed to plates seeded with both OP50 and the pathogenic *S. marcescens* bacteria for 24 hours. The mRNA fold changes for the candidate genes mostly did not conform to published data. Previous studies that indicate *Y116A8C.10* mRNA increases upon exposure to *S. marcescens*, contrary to what these data show (Sinha, et al., 2012). *egl-21* mRNA was also expected to rise, but failed to cluster in either direction (Engelmann et al., 2011). The decrease upon exposure of *daf-7* mRNA was consistent with published data (Taffoni & Pujol, 2015) (Figure 1.16). The ambiguity of mRNA levels in these experiments did not form a solid enough groundwork to pursue inquiries into 22G RNA responses.

Table 1.5
List of candidate genes
Candidate genes reportedly expressed in neuron only (wormbase.org WS276), differentially expressed in *sid-1* small RNA libraries compared to wild-type (L'Etoile 2015), bound to HRDE-1 in germline (Buckley 2012).

Candidate Gene	Function
mks-5	transmembrane glutamate receptor subunit
sol-2	lipid storage non-motile cilia assembly and protein localization to the cilia transition zone receptor localization to cilium
egl-21	required for normal synthesis of FMRFamide-like (FLP) and neuropeptide-like (NLP) peptides, and for normal egg-laying, locomotion, and defecation. Promotes acetylcholine release at neuromuscular junctions
daf-7	member of the transforming growth factor beta superfamily, functions as part of a signaling pathway that interprets environmental conditions to regulate energy-balance pathways that affect dauer larval formation, adult lifespan, fat metabolism, egg laying, pathogen avoidance behavior, and feeding behavior
mapk-15	mitogen activated protein kinase 15 ortholog, predicted to have ATP binding activity and protein kinase activity, involved in development and reproduction
Y116A8C.10	ortholog of human RABL3 (RAB, member of RAS oncogene family like 3), predicted to have GTP binding activity
trp-4	pore-forming subunit of a mechanosensitive TRPN (NOMPC) channel; TRP-4 is required for a mechanosensitive conductance in a ciliated mechanosensory neuron and, specifically, for stretch-receptor-mediated proprioception
arl-13	small ciliary G protein required for normal ciliary morphology and function and intraflagellar transport
mod-5	required for serotonin uptake by neurosecretory motor neurons and for the experience-dependent enhanced slowing response to food

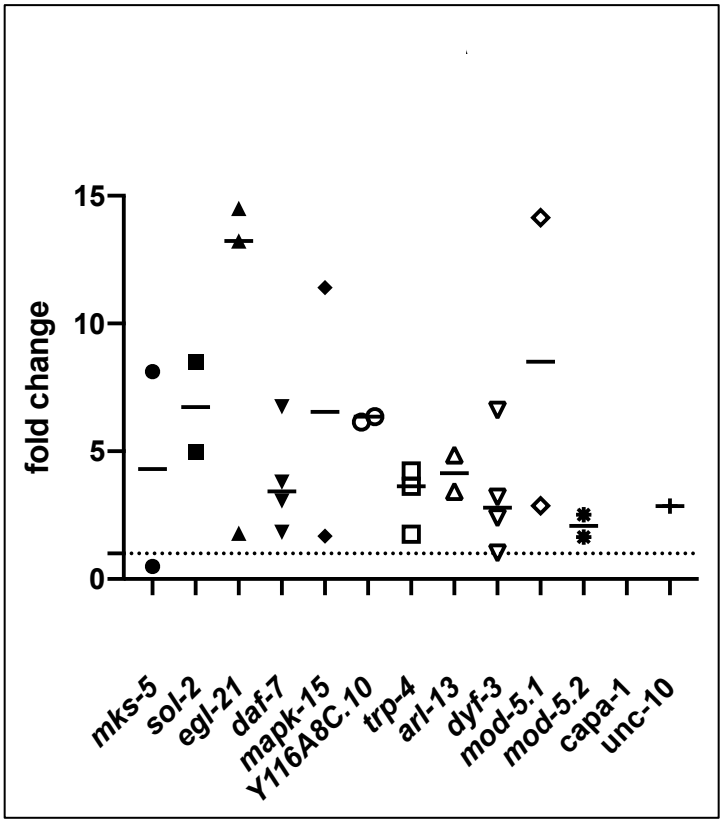

Figure 1.16
mRNA fold changes in starved vs well fed animals
qPCR quantification of mRNA of worm populations starved for 60 minutes vs well fed. These initial data did not cluster together and this line of inquiry was not pursued further. 2 biological replicates repeated 1-2 times.

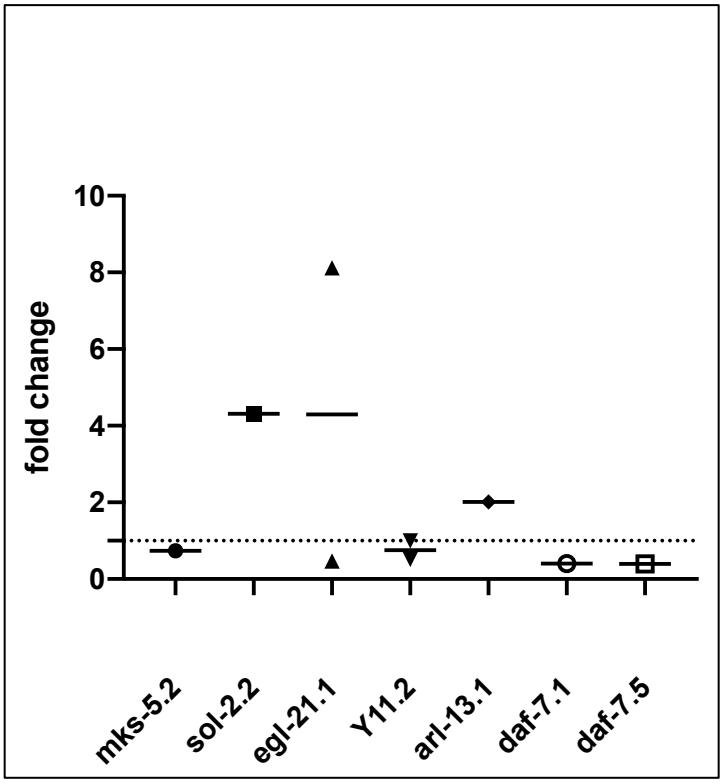

Figure 1.17
mRNA fold changes in healthy vs *S. marcescens* infected animals
qPCR quantification of mRNA of worm populations exposed to Serratia marcescens and Escherichia coli (OP50). 1 biological replicate repeated 1-2 times. Published data indicate *Y116A8C.10* mRNA increases upon exposure to *S. marcescens*, contrary to what these data show (Sinha, Rae, Iatsenko, & Sommer, 2012). *egl-21* mRNA was also expected to rise, contrary to these data (Engelmann et al., 2011). The decrease upon exposure of *daf-7* was consistent with published data (Taffoni & Pujol, 2015). This line of inquiry was not pursued further.

Current state of 22G RNA mediated transgenerational inheritance

Two recent studies have successfully documented biologically relevant transgenerational inheritance mediated by endo-siRNAs. The Rechavi lab at Tel Aviv University demonstrated that neuronal endo-siRNA species can be transmitted to the germline (Posner et al., 2019). Further, they found that *saeg-1*, a gene required for proper chemotaxis under stress, was downregulated in progeny by neuronally transmitted endo-siRNAs. They were able to identify

this candidate by restricting their small RNA libraries to neuron specific endo-siRNAs. They accomplished this in two ways: 1) using animals defective in the 22G biosynthetic pathway, *rde-4* (a dsRNA binding protein) mutants and rescuing RDE-4 under pan neuronal promoters and 2) FACS sorting neurons from these transgenic animals. This gave them a solid foundation on which to probe behaviorally relevant candidates. Further, by performing behavioral assays under high-temperature (25º) conditions, they were able to exacerbate behavioral defects and more clearly detect its transmission down generations.

The Murphy lab at Princeton University has determined that germline specific endo-siRNAs, Piwi-associated RNAs, are required for the transmission of learned avoidance to the pathogen *Pseudomonas aeruginosa* (Moore, Kaletsky, & Murphy, 2019). This avoidance behavior is mediated by an increase *daf-7* expression in ASI sensory neurons. When the P0 generation is exposed to *P. aeruginosa*, their progeny express higher levels of *daf-7 i*n ASI neurons, which directs them to avoid the pathogen, thereby conferring a fitness advantage. In progeny of pathogen exposed mutants defective in the Piwi/PRG-1 argonaute pathway, *daf-7* resembles that of uninfected animals. Not able to avoid the pathogenic fungus, their fitness suffers.

The field of mobile endo-siRNAs is dynamic and evolving. Ramifications extend far beyond the biology of *C. elegans*, and much remains unknown. Recent publications have pushed our understanding of how behaviors can be transmitted down generations. This work is vital to our understanding of how organisms perceive and react to the world. As these mechanisms become better characterized, we can more fully appreciate the effects of environmental stressors and potentially mediate how they manifest in future generations.

Chapter 1 References

Bargmann, C. I. (2006). Chemosensation in C. elegans. WormBook : the online review of C. elegans biology, 1-29. doi:10.1895/wormbook.1.123.1

Bargmann, C. I., Hartwieg, E., & Horvitz, H. R. (1993). Odorant-selective genes and neurons mediate olfaction in C. elegans. Cell, 74(3), 515-527. doi:10.1016/0092-8674(93)80053-h

Buckley, B. A., Burkhart, K. B., Gu, S. G., Spracklin, G., Kershner, A., Fritz, H., . . . Kennedy, S. (2012). A nuclear Argonaute promotes multigenerational epigenetic inheritance and germline immortality. Nature, 489(7416), 447-451. doi:10.1038/nature11352

Castel, S. E., & Martienssen, R. A. (2013). RNA interference in the nucleus: roles for small RNAs in transcription, epigenetics and beyond. Nat Rev Genet, 14(2), 100-112. doi:10.1038/nrg3355

Colbert, H. A., & Bargmann, C. I. (1995). Odorant-specific adaptation pathways generate olfactory plasticity in C. elegans. Neuron, 14(4), 803-812. doi:https://doi.org/10.1016/0896-6273(95)90224-4

Colbert, H. A., & Bargmann, C. I. (1997). Environmental signals modulate olfactory acuity, discrimination, and memory in Caenorhabditis elegans. Learning & Memory, 4(2), 179-191. doi:10.1101/lm.4.2.179

Dias, B. G., & Ressler, K. J. (2014). Parental olfactory experience influences behavior and neural structure in subsequent generations. Nature Neuroscience, 17(1), 89-96. doi:10.1038/nn.3594

Engelmann, I., Griffon, A., Tichit, L., Montañana-Sanchis, F., Wang, G., Reinke, V., . . . Ewbank, J. J. (2011). A Comprehensive Analysis of Gene Expression Changes Provoked

by Bacterial and Fungal Infection in C. elegans. PloS one, 6(5), e19055. doi:10.1371/journal.pone.0019055

Gu, W., Shirayama, M., Conte, D., Jr., Vasale, J., Batista, P. J., Claycomb, J. M., . . . Mello, C. C. (2009). Distinct argonaute-mediated 22G-RNA pathways direct genome surveillance in the C. elegans germline. Mol Cell, 36(2), 231-244. doi:10.1016/j.molcel.2009.09.020

Jose, A. M., Garcia, G. A., & Hunter, C. P. (2011). Two classes of silencing RNAs move between Caenorhabditis elegans tissues. Nature Structural & Molecular Biology, 18(11), 1184-1188. doi:10.1038/nsmb.2134

Juang, B.-T., Gu, C., Starnes, L., Palladino, F., Goga, A., Kennedy, S., & L'Etoile, Noelle D. (2013). Endogenous Nuclear RNAi Mediates Behavioral Adaptation to Odor. Cell, 154(5), 1010-1022. doi:https://doi.org/10.1016/j.cell.2013.08.006

L'Etoile, N. D., Coburn, C. M., Eastham, J., Kistler, A., Gallegos, G., & Bargmann, C. I. (2002). The Cyclic GMP-Dependent Protein Kinase EGL-4 Regulates Olfactory Adaptation in C. elegans. Neuron, 36(6), 1079-1089. doi:https://doi.org/10.1016/S0896-6273(02)01066-8

Moore, R. S., Kaletsky, R., & Murphy, C. T. (2019). Piwi/PRG-1 Argonaute and TGF-β Mediate Transgenerational Learned Pathogenic Avoidance. Cell, 177(7), 1827-1841.e1812. doi:https://doi.org/10.1016/j.cell.2019.05.024

Murayama, T., Toh, Y., Ohshima, Y., & Koga, M. (2005). The dyf-3 Gene Encodes a Novel Protein Required for Sensory Cilium Formation in Caenorhabditis elegans. *Journal of Molecular Biology, 346*(3), 677-687. doi:https://doi.org/10.1016/j.jmb.2004.12.005

Posner, R., Toker, I. A., Antonova, O., Star, E., Anava, S., Azmon, E., . . . Rechavi, O. (2019). Neuronal Small RNAs Control Behavior Transgenerationally. Cell, 177(7), 1814-1826.e1815. doi:https://doi.org/10.1016/j.cell.2019.04.029

Schulenburg, H., & Félix, M.-A. (2017). The Natural Biotic Environment of Caenorhabditis elegans. *Genetics, 206*(1), 55. doi:10.1534/genetics.116.195511

Sinha, A., Rae, R., Iatsenko, I., & Sommer, R. J. (2012). System wide analysis of the evolution of innate immunity in the nematode model species Caenorhabditis elegans and Pristionchus pacificus. PloS one, 7(9), e44255. doi:10.1371/journal.pone.0044255

Starich, T. A., Herman, R. K., Kari, C. K., Yeh, W. H., Schackwitz, W. S., Schuyler, M. W., . . . Riddle, D. L. (1995). Mutations affecting the chemosensory neurons of Caenorhabditis elegans. Genetics, 139(1), 171-188.

Taffoni, C., & Pujol, N. (2015). Mechanisms of innate immunity in C. elegans epidermis. Tissue barriers, 3(4), e1078432-e1078432. doi:10.1080/21688370.2015.1078432

Winston, W. M., Molodowitch, C., & Hunter, C. P. (2002). Systemic RNAi in C. elegans Requires the Putative Transmembrane Protein SID-1. Science, 295(5564), 2456. doi:10.1126/science.1068836

Worthy, S. E., Rojas, G. L., Taylor, C. J., & Glater, E. E. (2018). Identification of Odor Blend Used by Caenorhabditis elegans for Pathogen Recognition. *Chem Senses, 43*(3), 169-180. doi:10.1093/chemse/bjy001

Chapter 2

Transgenerational inheritance of behavior posits that stimuli detected by sensory neurons can combine with other input to generate behavior, and the underlying molecular mechanisms of that behavior transmit information to future generations, affecting how progeny interact with their environment. In essence, parental experience can be passed onto future generations enabling progeny to differently respond to specific challenges. Evidence of this phenomenon exists in many model organisms, from *C. elegans* to *Mus musculus* (Dias & Ressler, 2014) (Moore et al., 2019; Posner et al., 2019). These studies found that parental stress manifested as anatomical or behavioral changes in progeny and indicated that small and non-coding RNA (ncRNA) play a role in this process. Additional work has shown that artificially induced dsRNA in neurons is transmitted to and silences germline targets for multiple generations (Devanapally, Ravikumar, & Jose, 2015). Recent publications have documented mechanistic elements of inherited behavior, including identification of specific species of small RNA (Posner et al., 2019), however, it remains unknown how these RNA signals can exit neurons. One possible mechanism of neuronal RNA export lies in the processes of Rab-mediated canonical export. To explore this possibility, I designed a series of worm-based tools to monitor the spread of RNAi signals throughout the body.

Neuronal exocytosis

The nervous system of *C. elegans* consists of 302 neurons forming roughly 7000 chemical synapses (White, Southgate, Thomson, & Brenner, 1986). At these synapses, neurotransmitters are packaged into synaptic vesicles that mobilize to the presynaptic plasma membrane where they fuse with the plasma membrane upon a calcium signal trigger, releasing their contents into a synaptic cleft. Following this fusion, synaptic vesicles are recycled back into

the neuron for reuse. A wide array of proteins mediate this process, with many having overlapping functions (Richmond, 2007).

Highly conserved Rab proteins are the largest subgroup of the Ras family small GTPases (Stenmark & Olkkonen, 2001). In *C. elegans*, there are 25 members of the Rab family that regulate many aspects of intracellular synaptic vesicle trafficking and dynamics. In addition to mediating much of synaptic vesicle activity throughout the neuron, Rabs have been documented to mediate the trafficking and export extracellular vesicles (Savina, Vidal, & Colombo, 2002; Stenmark, 2009). This is of particular interest as many species of RNA, including micro RNA (miRNA) and other ncRNAs are known to populate extracellular vesicles (Kim, Abdelmohsen, Mustapic, Kapogiannis, & Gorospe, 2017).

Working with the Gallegos laboratory at California State University- East Bay, we were able to generate a series of neuronally expressed dominant negative mutations in several Rab species (Figure 2.1) (Table 2.1). These constructs were injected into worms, generating strains with motility defects ranging from twisted posture to reversal failures, but were otherwise healthy. Using these dominant negative Rab mutants, we sought to assess the role of specific Rab proteins in the export of exogenous RNA signal from neurons.

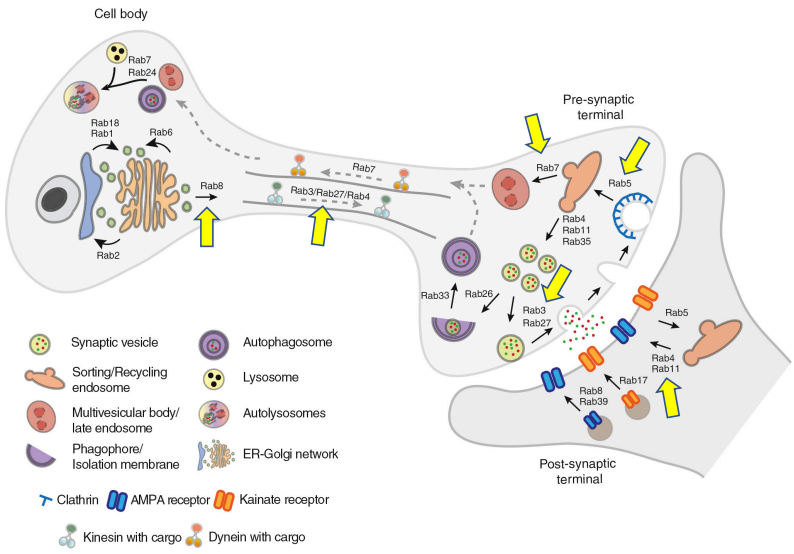

Figure 2.1
Rabs targeted in dominant negative screen
We generated a series of dominant negative Rab mutants that expressed in the pan-nueronal promoter pH20 (see Table 2.1). Relevant Rab proteins are indicated with yellow arrows. Adapted from (Guadagno & Progida, 2019).

Table 2.1
Rabs targeted in dominant negative screen.

Targeted Rab	Function
rab-3	tethering
rab-5	early endosome
rab-7	late endosome
rab-8	membrane trafficking
rab-10	membrane trafficking
rab-11.1	recycling
rab-27	regulated secretion

Designing a tissue-specific inducible dsRNA signal

Assessing the mechanism(s) of neuronal RNA export requires a robust tool. To identify components of this mechanism, this tool must meet three criteria: 1) an easily measured silencing response (indicating receipt of signal) 2) an indisputable source of neuronally generated dsRNA and 3) the ability to induce expression of dsRNA with no off-target effects. Foundational screens identified some of the genes required for RNAi mediated silencing spread by using the silencing of GFP as a readout (W. M. Winston, C. Molodowitch, & C. P. Hunter, 2002). To use GFP silencing as a readout here, expression of dsRNA GFP needs to be both restricted to neurons and inducible.

There is a long history of efforts to induce gene expression in model organisms, from heterologous Gal-4/UAS systems to heat-shock inducible promoters (Brand & Perrimon, 1993) (Barna, Csermely, & Vellai, 2018). With each new iteration of these tools, the dynamics, species applicability and spatial restriction improves. For our purposes, we required rapid onset and highly specific expression induced by an agent that does not affect the worm in any other way.

The repressive Q binary system was adapted for worms from Neurospora crassa as a tool for inducible gene expression (Wei, Potter, Luo, & Shen, 2012). This system is based on a transcriptional activator, QF, binding to a 16 base-pair sequence (termed QUAS) to express a downstream gene. Expression of genes downstream of the QUAS-site can be repressed by the transcriptional repressor, QS. Exposing transgenic animals to the non-toxic small molecule quinic acid de-represses QF and permits expression (Figure 2.2). This technique was modified to be tissue-specific in two ways 1) expressing QS and QF under different promoters and 2) by splitting the QF activating domain and binding domain into two constructs, allowing one to be expressed under a tissue-specific promoter.

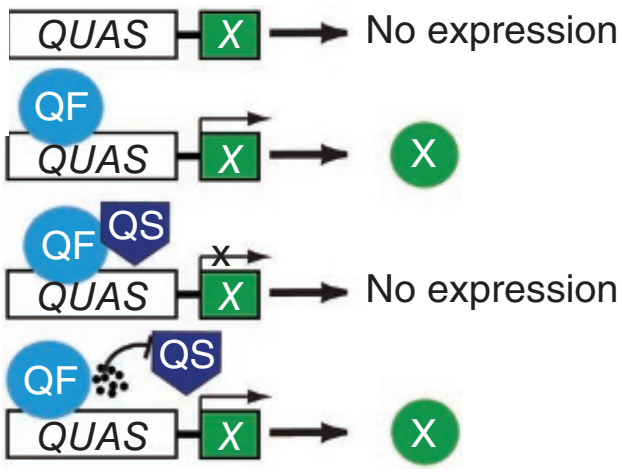

Figure 2.2
QF/QS repressive binary system
Transcriptional activator QF binds the 16 base-pair QUAS site to induce expression. Transcriptional repressor QS represses QF activated expression. Quinic acid acts to de-repress QS to activate expression of X. Adapted from (Wei et al., 2012).

While there is high tissue specificity in this tool, the response time is relatively slow (6 hours after quinic acid exposure to first detectable expression, 24 hours to full expression). Efforts to reduce the response time led to an advancement in this system, utilizing mammalian ligand binding domains. By fusing mammalian glucocorticoid receptor ligand binding domain (LBD) to the QF DNA binding domain (DBD) and activating domain (AD), the response time is dramatically reduced (Figure 2.3) (Monsalve, Yamamoto, & Ward, 2019). This system utilizes the mammalian steroid dexamethasone, which is not sensed by wild-type worms, further minimizing off-target effects.

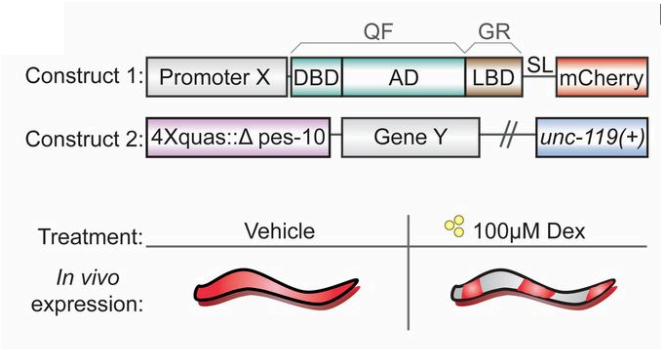

Figure 2.3
Dexamethasone-QF system
Under a tissue specific promoter, the QF domain (consisting of the DBD and AD of transcriptional activator QF) is fused to the LBD of mammalian glutocortocoid receptor. A minimalist global promoter is fused with 4X QUAS, the 16 base-pair binding site of transcriptional activator QF, and when activated expressed gene Y. 100uM dexamethasone, a steroid not sensed by wild-type worms, is sufficient to induce expression of gene Y in as little as 1 hour. Adapted from (Monsalve et al., 2019).

Rigid tissue specificity paired with rapid onset expression presented an ideal tool for exploring export mechanisms of exogenously produced dsRNA. Using the modified dexamethasone-QUAS system, GFP dsRNA expression could be induced in neurons, with the dynamics of silencing in somatic and germline cells serving as a readout for the rate of RNAi signal spread.

With neuronal export as the focus, the GFP dsRNA would need to be only expressed in the neurons. To accomplish this, I cloned a pan-neuronal promoter, pH20, into the first construct of the dexamethasone-QUAS system (*pH20:QF-GR::SL2::mCherry*) (Figure 2.4). Correct expression was verified by microscopy (Figure 2.5).

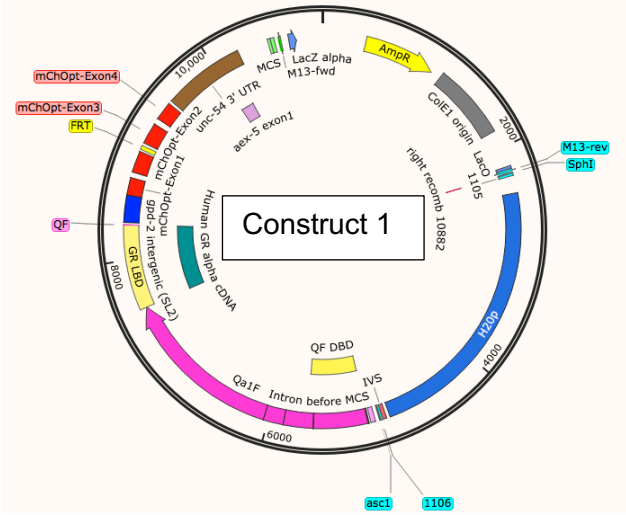

Figure 2.4
Map of construct 1: *pH20:QF-GR::SL2::mCherry*
Plasmid adapted from pGM32 (Monsalve et al., 2019)

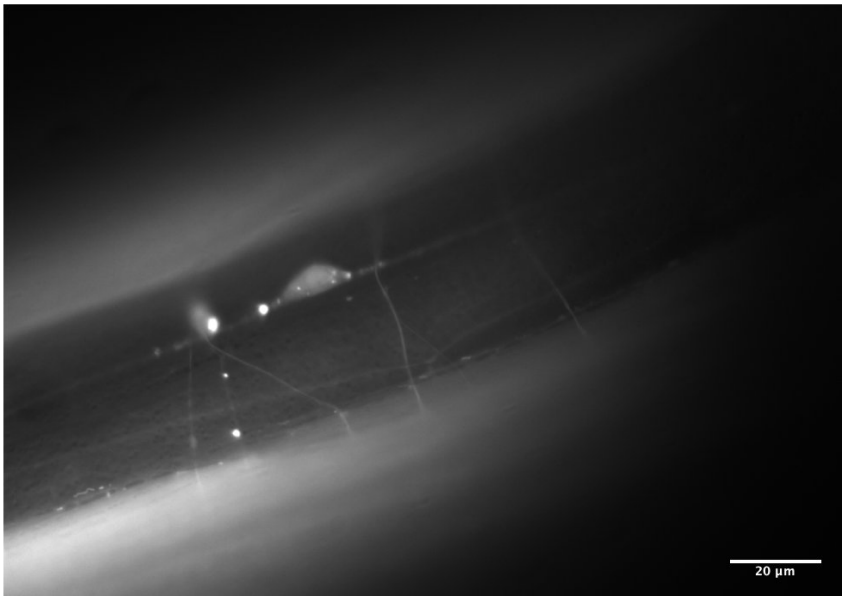

Figure 2.5
pH20:QF-GR::SL2::mCherry expression.
A day one adult worm expressing *pH20:QF-GR::SL2::mCherry*. Imaged on a Zeiss AxioPlan 2ie MOT motorized upright fluorescent microscope. mCherry is seen expressed in all neurons.

I cloned the second construct using the minimalist fused 5X QUAS Δ*pes-10* promoter to express a hairpin GFP. The hairpin GFP sequence was acquired from the Hunter and Jose labs and was used in the original screens identifying mutants in the RNAi pathway (W. M. Winston et al., 2002) (Figure 2.6).

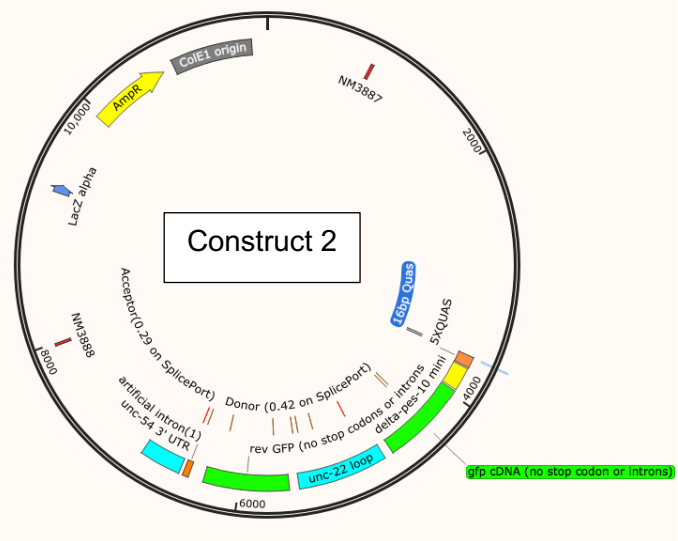

Figure 2.6
Map of construct 2: *5XQUAS-*Δ*pes-10::hpGFP*
Plasmid adapted from pGM34 (Monsalve et al., 2019)

We were able to induce some expression of GFP in the control strain KRY569 (N2, *Is(pro-1p::GF-GR::SL::mCherry); Is(quas::GFP)*) after 2 hours on 100uM dexamethasone plates (Figure 2.7). This integrated line expresses mCherry constitutively under a global promoter. GFP is expressed upon QF activation following dexamethasone treatment. First GFP expression is seen in two dots in the head region (indicated with arrow).

I injected our modified constructs into animals expressing *psur-5::GFP(NLS)* to generate non-integrated strains. However, transgenic positive animals failed to silence GFP 24 hours following a 6 hour treatment on dexamethasone plates (Figure 2.8). The constitutively expressed first construct (QF-GR) can be identified in neurons using a red channel. GFP expression

remains unchanged between transgenic positive and negative animals 24 hours following a 6 hour exposure to 100uM dexamethasone.

Figure 2.7
Induction of dexamethasone-induced control strain
Strain KRY569 (N2, *Is(pro-1p::GF-GR::SL::mCherry); Is(quas::GFP)*) after 2 hours on 100uM dexamethasone plate. mCherry is constitutively expressed, GFP is induced by dexatmethasone treatment. A) Brightfield. B) Red channel, inverted. C) Green channel, inverted. Arrow indicates early expression of GFP.

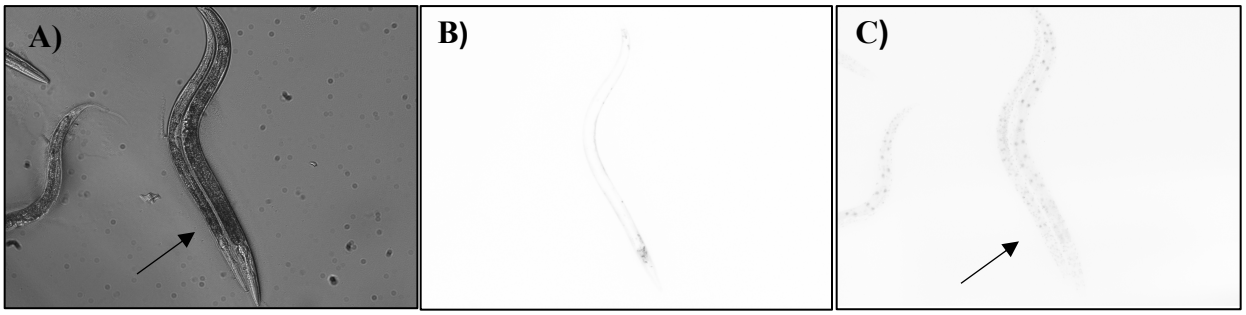

Figure 2.8
6 hour dexamethasone treatment of inducible GFP hairpin strain
Animals expressing both constructs fail to silence GFP 24 hours after a 6 hour 100uM dexamethasone treatment. A) Brightfield, transgenic positive animal indicated with arrow. B) Red channel, mCherry is constitutively expressed under the H20 promoter, inverted. C) Green channel, transgenic positive animal indicated with arrow, inverted. GFP expression is the same for transgenic positive and negative animals, indicating a failure to silence.

To assess if the inducible construct was failing to express the hairpin or if the hairpin itself was failing to silence GFP, I probed the mRNA content of transgenic positive vs transgenic negative induced animals. I designed 6 primers sets probing the junction between the GFP and unc-22 loop sequences. If the hairpin was expressed but failing to silence, there would be detectable signal only in animals carrying the array. However, I was unable to detect any changes between the transgenic and non-transgenic populations, indicating the hairpin is likely not expressed in this strain (Figure 2.9).

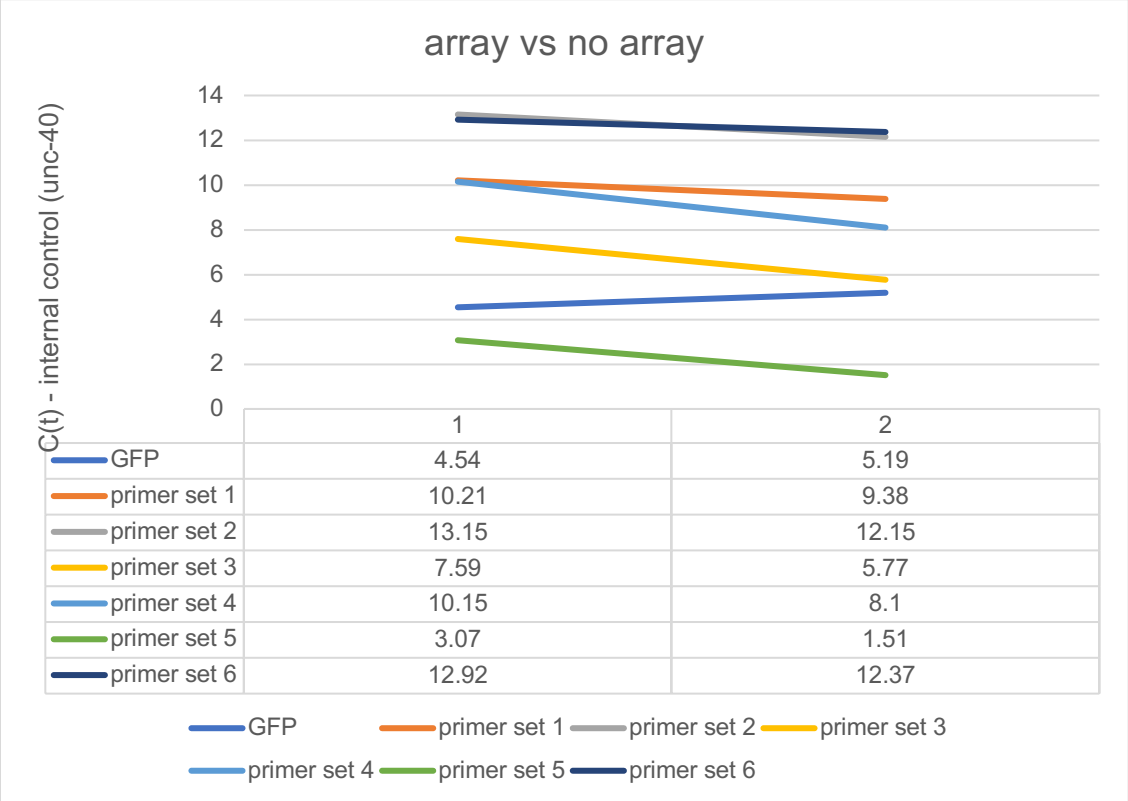

	1	2
GFP	4.54	5.19
primer set 1	10.21	9.38
primer set 2	13.15	12.15
primer set 3	7.59	5.77
primer set 4	10.15	8.1
primer set 5	3.07	1.51
primer set 6	12.92	12.37

Figure 2.9
mRNA probe of GFP hairpin in induced animals
6 primer sets targeting the junction between GFP and *unc-22* loop sequences failed to detect measurable differences between transgenic positive and transgenic negative animals exposed to dexamethasone. A control primer pair measuring GFP mRNA also demonstrates a failure of GFP to silence. All C(t) values were normalized to an unc-40 control primer set. N=1 biological replicate.

It is possible that the failure of these inducible constructs to express a GFP hairpin lies in the relatively complicated structure of the hairpin. To address this, I injected the *pH20 QF-GR* construct along with two inducible QUAS constructs, one expressing the forward sequence of GFP and one expressing the reverse sequence of GFP at a 2:1:1 ratio. Upon exposure to dexamethasone, QF would be expressed in the neurons, and then bind to the QUAS sequence driving both positive and negative sequences of GFP. The positive and negative strands of RNA would associate to form GFP dsRNA, which would then engage in RNAi. However, upon induction, no silencing was observed. Contrary to expectations, GFP expression emerged in the neurons, suggesting the constructs were responding to dexamethasone but not forming dsRNA.

Chapter 2 References

Barna, J., Csermely, P., & Vellai, T. (2018). Roles of heat shock factor 1 beyond the heat shock response. Cellular and Molecular Life Sciences, 75(16), 2897-2916. doi:10.1007/s00018-018-2836-6

Brand, A. H., & Perrimon, N. (1993). Targeted gene expression as a means of altering cell fates and generating dominant phenotypes. Development, 118(2), 401-415.

Devanapally, S., Ravikumar, S., & Jose, A. M. (2015). Double-stranded RNA made in C. elegans neurons can enter the germline and cause transgenerational gene silencing. Proc Natl Acad Sci U S A, 112(7), 2133-2138. doi:10.1073/pnas.1423333112

Dias, B. G., & Ressler, K. J. (2014). Parental olfactory experience influences behavior and neural structure in subsequent generations. Nature Neuroscience, 17(1), 89-96. doi:10.1038/nn.3594

Guadagno, N. A., & Progida, C. (2019). Rab GTPases: Switching to Human Diseases. Cells, 8(8), 909. Retrieved from https://www.mdpi.com/2073-4409/8/8/909

Kim, K. M., Abdelmohsen, K., Mustapic, M., Kapogiannis, D., & Gorospe, M. (2017). RNA in extracellular vesicles. WIREs RNA, 8(4), e1413. doi:10.1002/wrna.1413

Monsalve, G. C., Yamamoto, K. R., & Ward, J. D. (2019). A New Tool for Inducible Gene Expression in <em>Caenorhabditis elegans</em&gt. Genetics, 211(2), 419. doi:10.1534/genetics.118.301705

Moore, R. S., Kaletsky, R., & Murphy, C. T. (2019). Piwi/PRG-1 Argonaute and TGF-β Mediate Transgenerational Learned Pathogenic Avoidance. Cell, 177(7), 1827-1841.e1812. doi:https://doi.org/10.1016/j.cell.2019.05.024

Posner, R., Toker, I. A., Antonova, O., Star, E., Anava, S., Azmon, E., . . . Rechavi, O. (2019). Neuronal Small RNAs Control Behavior Transgenerationally. Cell, 177(7), 1814-1826.e1815. doi:https://doi.org/10.1016/j.cell.2019.04.029

Richmond, J. (2007). Synaptic function. *Wormbook.* The *C. elegans* Research Community, doi/10.1895/wormbook1.69.1

Savina, A., Vidal, M., & Colombo, M. I. (2002). The exosome pathway in K562 cells is regulated by Rab11. Journal of Cell Science, 115(12), 2505. Retrieved from http://jcs.biologists.org/content/115/12/2505.abstract

Stenmark, H. (2009). Rab GTPases as coordinators of vesicle traffic. Nature Reviews Molecular Cell Biology, 10(8), 513-525. doi:10.1038/nrm2728

Stenmark, H., & Olkkonen, V. M. (2001). The Rab GTPase family. Genome Biology, 2(5), reviews3007.3001. doi:10.1186/gb-2001-2-5-reviews3007

Wei, X., Potter, C. J., Luo, L., & Shen, K. (2012). Controlling gene expression with the Q repressible binary expression system in Caenorhabditis elegans. Nature Methods, 9(4), 391-395. doi:10.1038/nmeth.1929

White, J. G., Southgate, E., Thomson, J. N., & Brenner, S. (1986). The structure of the nervous system of the nematode Caenorhabditis elegans. Philos Trans R Soc Lond B Biol Sci, 314(1165), 1-340. doi:10.1098/rstb.1986.0056

Winston, W. M., Molodowitch, C., & Hunter, C. P. (2002). Systemic RNAi in C. elegans requires the putative transmembrane protein SID-1. Science, 295(5564), 2456-2459. doi:10.1126/science.1068836

Chapter 3

For decades, RNAi has been a foundational tool in the field of *C. elegans* and beyond. It has illuminated diverse biology ranging from metabolism to meiosis by enabling the control of gene expression outside of genetic mutants. However, the biology of RNAi is a fertile course of study in its own right. RNA biology infuses all life on earth and exogenous RNAi allows for the controlled manipulation of RNA in living creatures.

RNAi triggered silencing occurs upon the introduction of dsRNA to a worm, by injection, feeding or transgenic expression. The silencing response triggered by the presence of dsRNA likely evolved as a mechanism of viral immunity. Single stranded RNA viruses replicate in the animal, forming viral dsRNA species and triggering a response to identify and degrade target sequence (Ermolaeva & Schumacher, 2014). In an experimental setting, worms can be injected with or fed *E. coli* expressing dsRNA species with the goal of knocking down a particular gene's function. The efficacy of RNAi is rooted in two aspects, amplification and spread. In a tissue of origin, dsRNA is processed by a variety of well characterized proteins to amplify intermediary species that degrade mRNA and are directed to a gene to engage in gene silencing. As this is proceeding in the origin tissue, a silencing signal exits and spreads into the rest of the worm, further engaging in gene silencing.

The mechanisms by which RNAi signals enter a cell are well documented (Figure 3.1) (Rocheleau, 2012). SID-2 is a transmembrane protein expressed at the intestinal lumen and is required for the uptake of environmental (feeding) RNAi (Winston, Sutherlin, Wright, Feinberg, & Hunter, 2007). SID-1 is dsRNA import channel expressed in all cells, except for neurons, and is required for the import of RNAi spreading signals (Feinberg & Hunter, 2003; Shih, Fitzgerald,

Sutherlin, & Hunter, 2009; W. M. Winston et al., 2002). SID-4 has been reported to be an import protein that genetically interacts with the signaling protein SID-3 (Bhatia & Hunter, 2019).

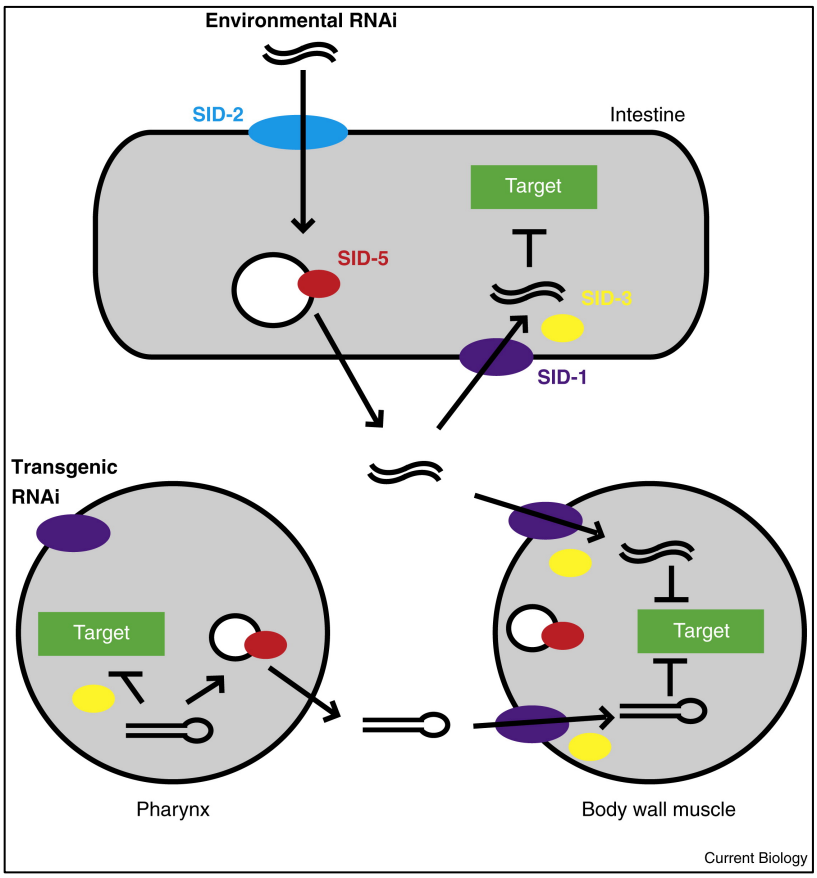

Figure 3.1
dsRNA transport in *C. elegans*
Environmental RNAi is imported into intestinal cells via the SID-2 channel. SID-1 serves as the import channel for all other cells, and additionally acts in intestinal cells to uptake internalized RNAi signals. SID-5 is the only known participant in RNAi export, and is a transmembrane protein localized to the late endosome. SID-4 (not shown) may also act in import and interacts with SID-3.
Adapted from (Rocheleau, 2012).

While several members of the import pathway are well defined, there is only one documented export protein. SID-5 is a transmembrane protein that is found in late endosomes required for the export of RNAi signals (Hinas, Wright, & Hunter, 2012). Further, SID-1 and SID-5 are necessary for efficient transmission of parental RNAi to embryos (Wang & Hunter, 2017). SID-5 is a relatively small single-pass transmembrane protein, with known homologs within the Caenorhabditis genus. However, at 67 amino acids in length, the sensitivity of protein homology search algorithms is reduced, so it is possible that forms of this protein exist in other organisms (Hinas et al., 2012).

Immunohistochemistry experiments reveal some colocalization between SID-5 and other late endosomal proteins RAB-7 and LMP-1 (Hinas et al., 2012). Further indicating a role in RNAi signal transport, 5EU labeled dsRNA has been shown to occasionally inhabit RAB-7 containing vesicles in embryonic cells (Wang & Hunter, 2017). These studies aside, there is a relative dearth of information in the RNA export field. There are gaps in both the identification of export pathway members as well as factors that may influence the process.

Secretory autophagy and RNAi spread

Classical autophagy is the process by which cells dispose of intracellular waste by encapsulating them in vesicles and degrading its contents. Autophagy is vital to the overall health of a cell or organism, acting as quality control while salvaging key metabolites (Kaur & Debnath, 2015). However, the autophagic pathway is not restricted to this one role. Secretory autophagy is a process by which vesicles entering into the autophagic pathway are diverted from a lysosomal degradative state to the plasma membrane for export. In many organisms, this unconventional secretion is the export mechanism for many species of cargo, including proteins

lacking a N-terminal signal sequence (e.g. yeast Acb1) and various inflammatory mediators (e.g. mammalian IL-1ß and IL-18) (Figure 3.2) (Cadwell & Debnath, 2017).

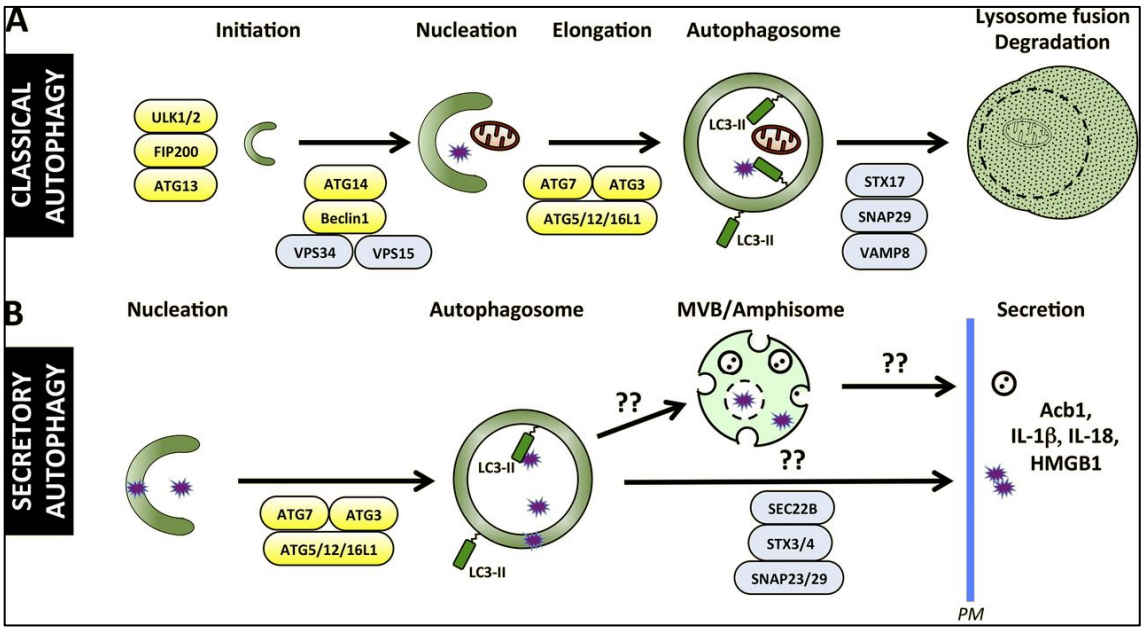

Figure 3.2
Classical vs secretory autophagy
Classical autophagy is the mechanism by which cells can degrade defective cellular components, such as misfolded proteins. A vesicle initiates and elongates to encapsulate cargo, which is then directed to the lysosome for enzymatic degradation. Secretory autophagy undergoes similar initiation and elongation, but the autophagasome is redirected to the plasma membrane where contents are expelled from the cell. Adapted from Cadwell and Debnath, 2017.

In *C. elegans*, LGG-1 (known as Atg8/LC3 elsewhere) is recruited to the forming autophagasome during elongation. Tagged LGG-1 is a widespread tool in monitoring autophagic flux microscopically (Chen, Scarcelli, & Legouis, 2017). LGG-1 is also known to directly interact with the RNA induced silencing complex (RISC) component AIN-1 (a GW182 homolog) (Zhang & Zhang, 2013) (Figure 3.3). This interaction indicates that RNA may be present in the autophagic pathway, with secretory autophagy a candidate for RNA export.

To probe if secretory autophagy is involved in worm-wide spread of RNAi silencing signals, I set out to assess feeding RNAi spread in animals defective in the autophagic pathway. ATG-3 and ATG-7 are E2 and E1 ubiquitin-like enzymes, respectively, involved in LGG-1 lipidation and membrane elongation (Figure 3.3). I crossed wild-type, *atg-3 (bp412)* and *atg-7 (bp411)* with stably expressing mos1-mediated single copy insertion (moSCI) GFP lines to generate a readout for GFP silencing. By comparing the rate of GFP silencing in these three strains, I sought to determine if secretory autophagy is responsible for some RNA export.

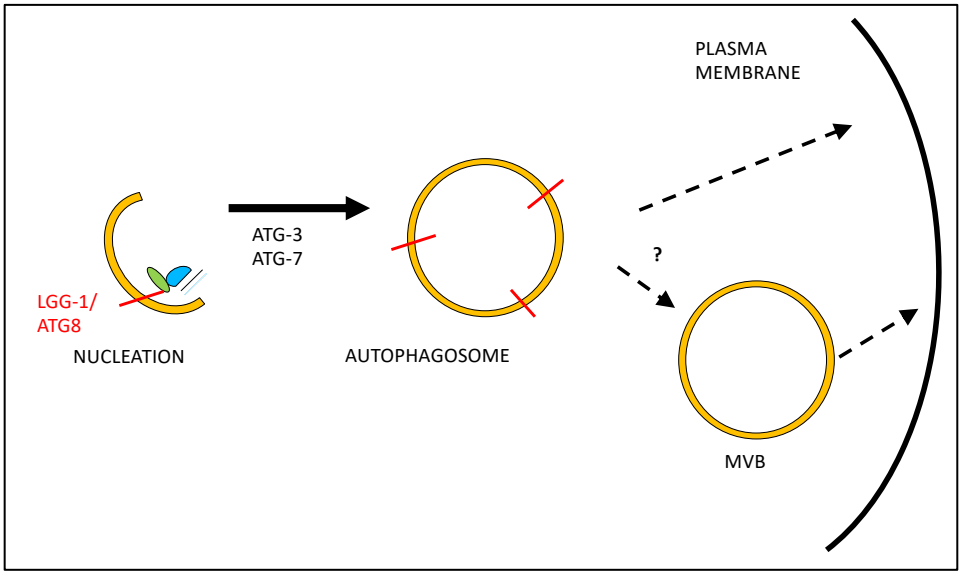

Figure 3.3
Secretory autophagy as a model for RNA export
The nucleating autophagosome recruits LGG-1(red) that directly interacts with RISC components AIN-1 (green) and argonautes (blue). ATG-3 and ATG-7 are E2 and E1 ubiquitin-like enzymes, respectively, involved in LGG-1 lipidation and membrane elongation. The autophagasome containing RISC components are then potentially redirected to the plasma membrane for export.

atg-3 (*bp412*) and *atg-7* (*bp411*) mutant strains each carry a point mutation that yields a mild phenotype (Tian et al., 2010). Animals have mild aging, fecundity and size defects, but otherwise appear wild-type (Figure 3.4). Efficient autophagy is required for apoptotic cell clearance during development. When autophagy is defective, a rise in cell corpse numbers is observed in developing embryos. This phenotype is helpful for determining defects in the autophagy pathway (Huang, Jia, Wang, Zhou, & Levine, 2013). DIC imaging reveals increased cell corpse numbers in both *atg-3* and *atg-7* mutants during development (Figure 3.4).

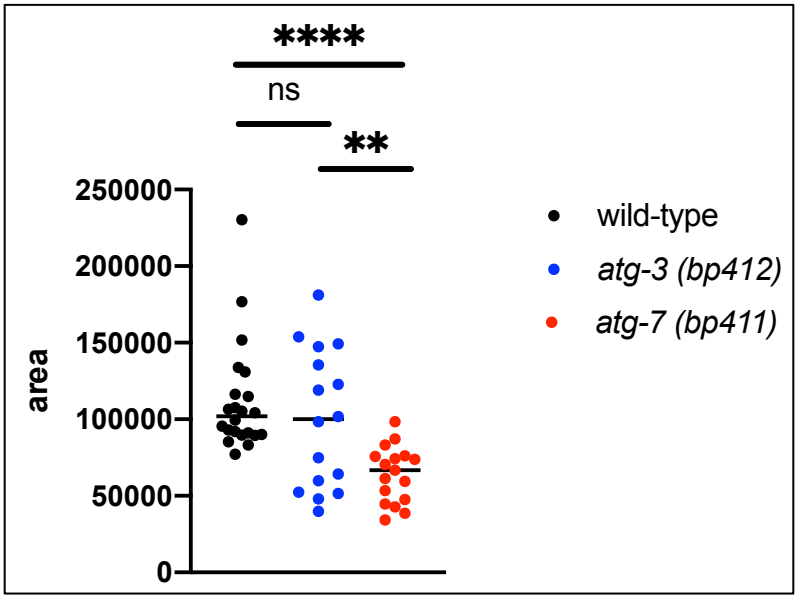

Figure 3.4
Relative sizes of *atg-3* and *atg-7* mutants, compared with wild-type
ROI areas of experimental animals. ROI is defined as anterior to vulva in L4 animals, single median plane. Unpaired T test determined no statistical significance between wild-type and atg-3 animals, p=<.0001 between wild-type and *atg-7* mutants, and p=.005 between *atg-3* and *atg-7* mutants.

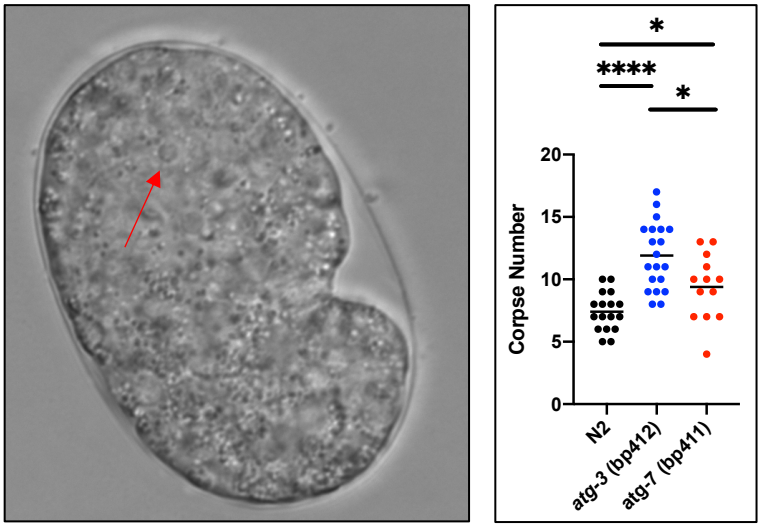

Figure 3.5
Cell corpse engulfment
Cell corpse engulfment at embryonic bean stage, 6 hours post fertilization. A) Red arrow indicates corpse engulfment. B) Number of corpses are greater in atg-3 mutant animals (unpaired T test, p=<0.0001) and atg-7 mutant animals (p=0.0156) compared to wild-type. Number of corpses are greater in *atg-3* mutant animals than *atg-7* mutant animals (p=0.0127).

Qualified assessment of silencing in autophagy mutants

To assess the capacity of *atg-3* and *atg-7* mutant strains to spread RNAi signal, I employed feeding RNAi mediated GFP silencing. By design, the original forward genetic screen that identified the initial systemic RNA interference defective (SID) mutants used a single end-point, with focus on more dramatic phenotypes (W. M. Winston et al., 2002). In order to capture any variations in the dynamics of silencing, I wanted to take a more longitudinal look. I included N2 wild-type worms as a positive control for RNAi silencing signal spread and *sid-5* mutant worms as a negative control. Synchronized eggs were laid on RNAi permissive nematode growth medium (NGM) plates containing ampicillin and isopropyl β-D-thiogalactoside (IPTG) and seeded with E. coli (HT115) expressing either empty vector or dsRNA targeting GFP. Mutant strains and wild-type worms, all carrying *pmyo-3::GFP* and/or *pelt-2::GFP* transgenes were left

to develop for 4 days, with measurements taken every day with a particular focus on day 2 (L4) and day 3 (adult).

Initial experiments were carried out in a qualitative fashion. Analysis was restricted to worms expressing GFP (NLS) in muscle only (*pmyo-3::GFP*). Levels of expression were binned into 4 categories 1) no silencing, or 100% GFP expression 2) mostly expressed, or >50% GFP expression 3) mostly silenced, or <50% GFP expression and 4) completely silenced, or 0% GFP expression. (Figure 3.6).

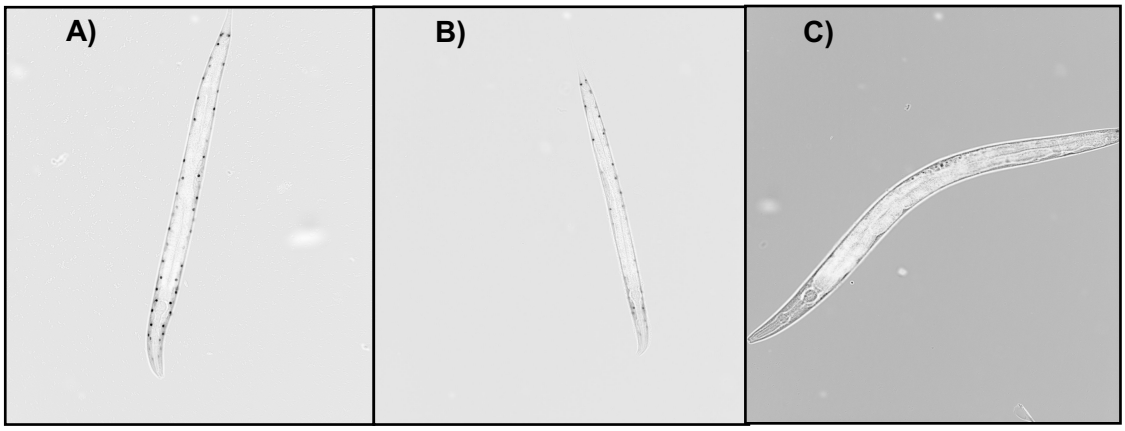

Figure 3.6
Qualitative categories of RNAi mediated silencing in MYO-3:GFP animals
Inverted fluorescent images. Assessment of number of GFP positive nuclei/ A) Full GFP expression, 100% expressed B) Mostly expressed, >50% GFP C) Mostly silenced, <50% GFP. Fully silenced, 0% GFP not shown.

After growing for 2 days on bacteria expressing dsRNA targeting GFP, N2 wild-type animals were nearly completely silenced when compared to siblings grown on empty vector bacteria. *atg-3* animals displayed a similar degree of silencing when compared to wild-type. *atg-7* silenced GFP to a lesser degree than wild-type but engaged in more silencing than *sid-5* animals. *sid-5* animals largely failed to silence GFP by day 2 (Figure 3.7).

By day 3, the autophagy mutant strains have both achieved wild-type levels of GFP silencing in muscle cell nuclei. *sid-5* animals continue to exhibit defective silencing compared to wild-type and autophagy mutants. The reduced silencing observed in *atg-7* mutants on day 2 achieves wild-type silencing by day 3 (Figure 3.8).

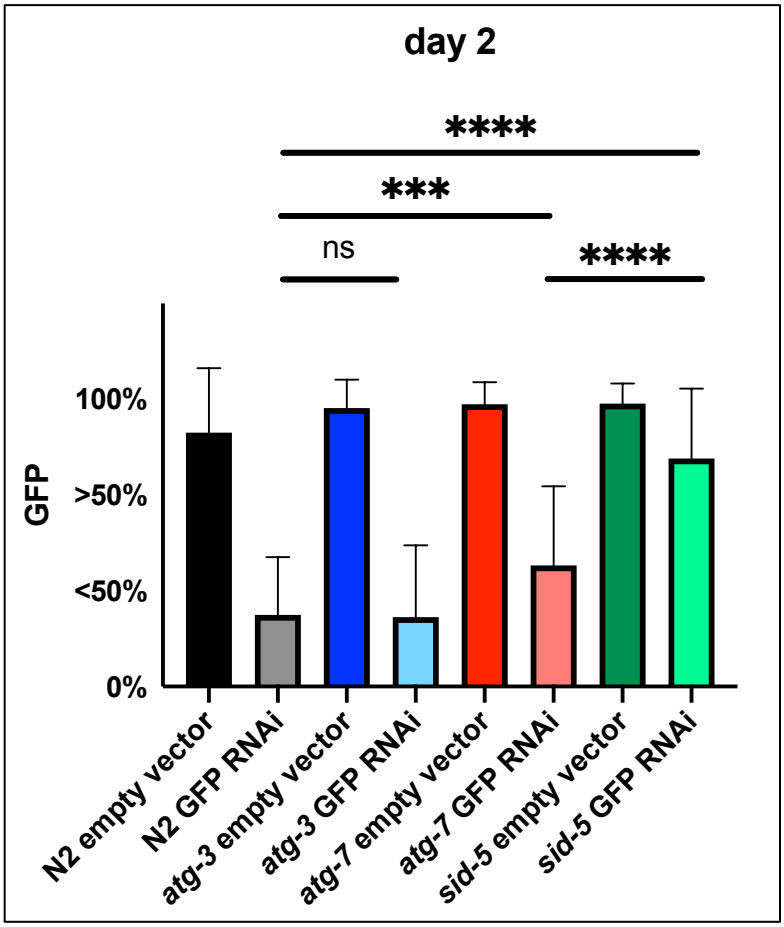

Figure 3.7
Qualitative silencing of GFP expressed in muscle nuclei on day 2
N2 animals exposed to bacteria expressing empty vector in black, expressing dsRNA targeting GFP in grey. *atg-3* animals exposed to bacteria expressing empty vector in dark blue, expressing dsRNA targeting GFP in light blue. *atg-7* animals exposed to bacteria expressing empty vector in deep red, expressing dsRNA targeting GFP in pink. *sid-5* animals exposed to bacteria expressing empty vector in dark green, expressing dsRNA targeting GFP in light green. All but *sid-5* animals silenced GFP when exposed to bacteria expressing dsRNA targeting GFP by day 2. N2 wild-type animals silenced GFP at the same rate as *atg-3* mutants. *atg-7* mutants silenced GFP to a lesser degree, compared with wild-type (unpaired t test, $p=0.0008$) and a greater degree when compared to sid-5 ($p<0.00001$). The negative control for GFP silencing, *sid-5* failed to silence compared with the positive control for GFP silencing, N2 wild-type ($p<0.00001$).

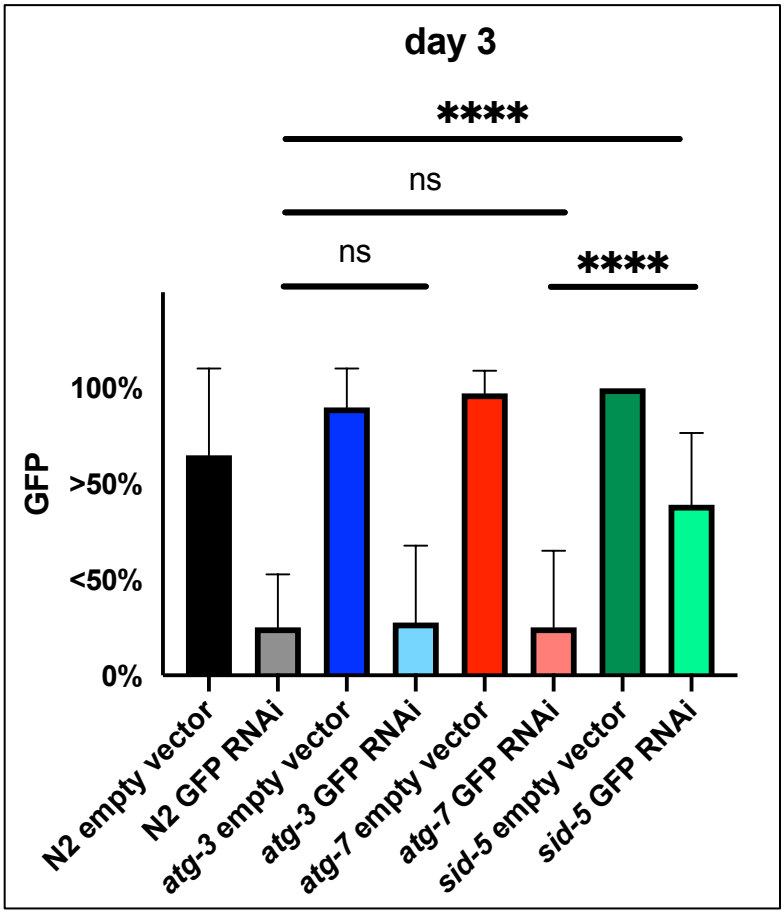

Figure 3.8
Qualitative silencing of GFP expressed in muscle nuclei on day 3.
N2 animals exposed to bacteria expressing empty vector in black, expressing dsRNA targeting GFP in grey. *atg-3* animals exposed to bacteria expressing empty vector in dark blue, expressing dsRNA targeting GFP in light blue. *atg-7* animals exposed to bacteria expressing empty vector in deep red, expressing dsRNA targeting GFP in pink. *sid-5* animals exposed to bacteria expressing empty vector in dark green, expressing dsRNA targeting GFP in light green. Autophagy mutants silence to the same degree as N2 wild-type by day 3. *sid-5* silences to a lesser degree compared to both N2 wild-type (unpaired t test, $p < 0.00001$) and *atg-7* ($p < 0.00001$).

Quantified assessment of silencing in autophagy mutants

Though the previous qualified assessments were blinded, it was necessary to employ a more non-biased, quantitative approach. To accomplish this, the experimental design could remain the same if coupled with a more precise analysis. Working with individuals among populations, I imaged each animal and defined the ROI as the anterior half of the animal, using the vulva as a marker, when developmentally available. Using this method, I was also able to define tissue specificity, separating the intestine (using GFP driven by the *elt-2* promoter) and muscle cells (*myo-3* promoter). This is helpful in determining if autophagy is involved in autonomous RNAi silencing or spread of RNAi silencing, as well as revealing more subtle phenotypes.

All three genotypes tested, N2 wild-type, *atg-3*, and *atg-7* significantly silenced when fed bacteria expressing dsRNA targeting GFP compared with siblings fed bacteria expressing an empty vector. Partial silencing was accomplished on day 2, with complete silencing achieved on day 3 (Figures 3.9-10). Restricting analysis to animals exposed to dsRNA targeting GFP, no change was observed in either tissue in either of the mutants, compared to wild-type on day 2 (Figure 3.11). On day 3, there was a slight reduction in GFP silencing in the gut of *atg-3* mutants, compared to wild-type. However, gut autofluorescence becomes a confounding factor in these adult animals (Figure 3.12).

These results taken together indicate that *atg-3* (bp412) and *atg-7* (bp411) engage in relatively normal systemic RNAi spreading. Pilot experiments had suggested a potential defect, but the phenotype dissipated as replicates increased. However, these data do not rule out the possibility that secretory autophagy is involved in the export of biologically active RNA species. Both autophagy mutants present a mild phenotype. Conclusive evidence in either direction

should be based on animals demonstrating a stronger defect. Such strains exist but are not freely available.

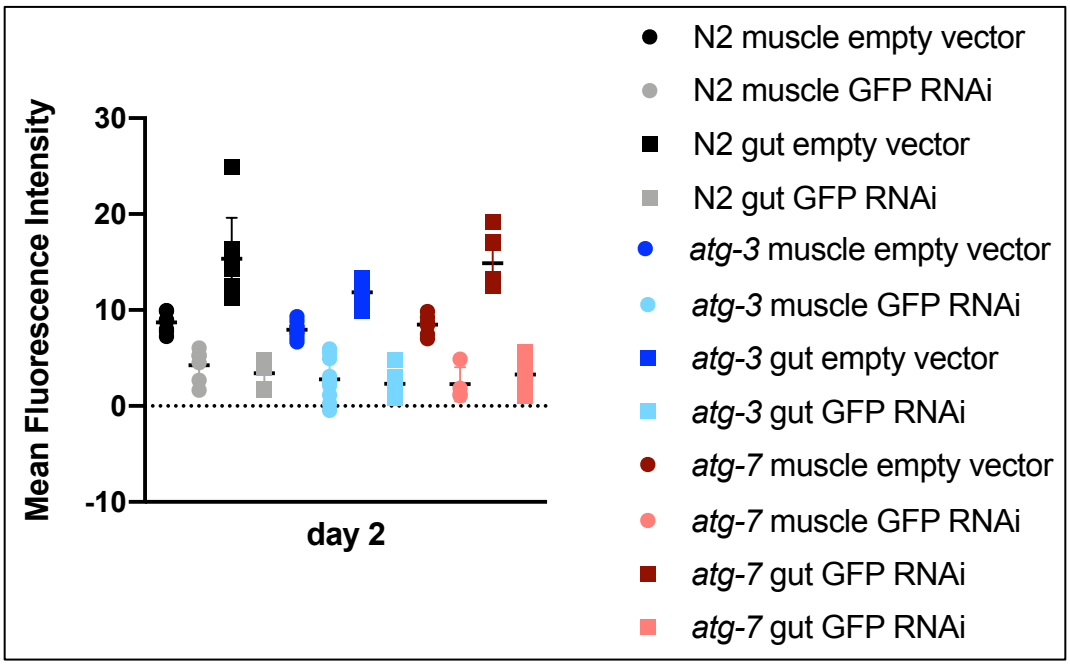

Figure 3.9
Quantification of GFP silencing in muscle and gut on day 2 of RNAi treatment
N2 animals exposed to bacteria expressing empty vector in black, expressing dsRNA targeting GFP in grey. *atg-3* animals exposed to bacteria expressing empty vector in dark blue, expressing dsRNA targeting GFP in light blue. *atg-7* animals exposed to bacteria expressing empty vector in deep red, expressing dsRNA targeting GFP in pink. Muscle data points are circles. Gut data points are squares. All animals significantly silenced when exposed to bacteria expressing dsRNA targeting GFP. Unpaired t test, $p<0.0001$

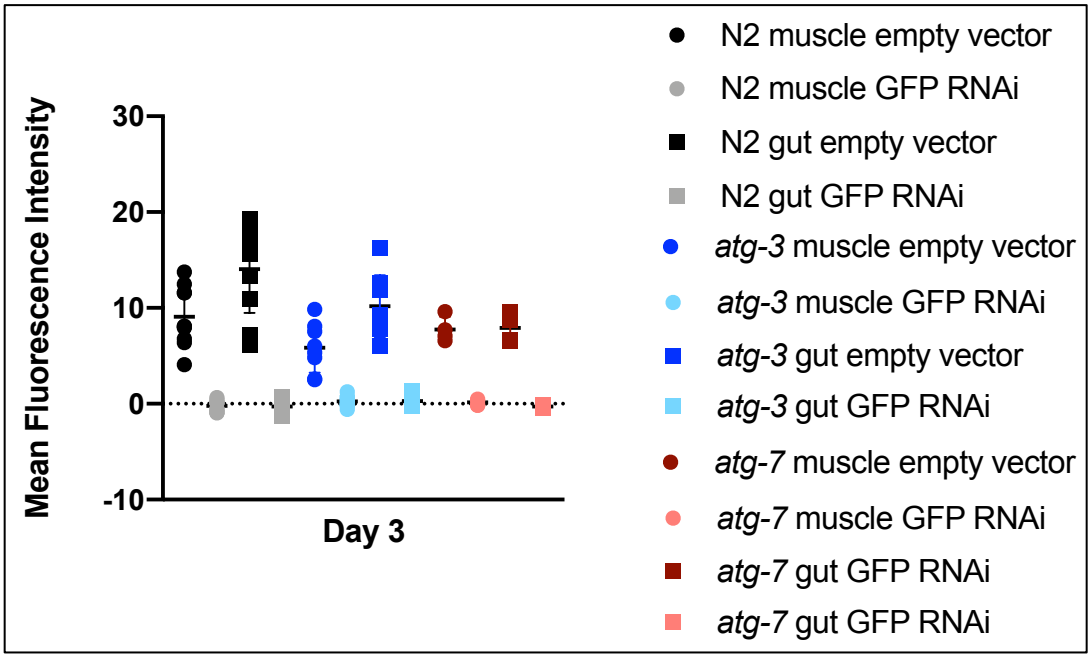

Figure 3.10
Quantification of GFP silencing in muscle and gut on day 3 of RNAi treatment
N2 animals exposed to bacteria expressing empty vector in black, expressing dsRNA targeting GFP in grey. *atg-3* animals exposed to bacteria expressing empty vector in dark blue, expressing dsRNA targeting GFP in light blue. *atg-7* animals exposed to bacteria expressing empty vector in deep red, expressing dsRNA targeting GFP in pink. Muscle data points are circles. Gut data points are squares. All animals significantly silenced when exposed to bacteria expressing dsRNA targeting GFP. Unpaired t test, $p<0.0001$

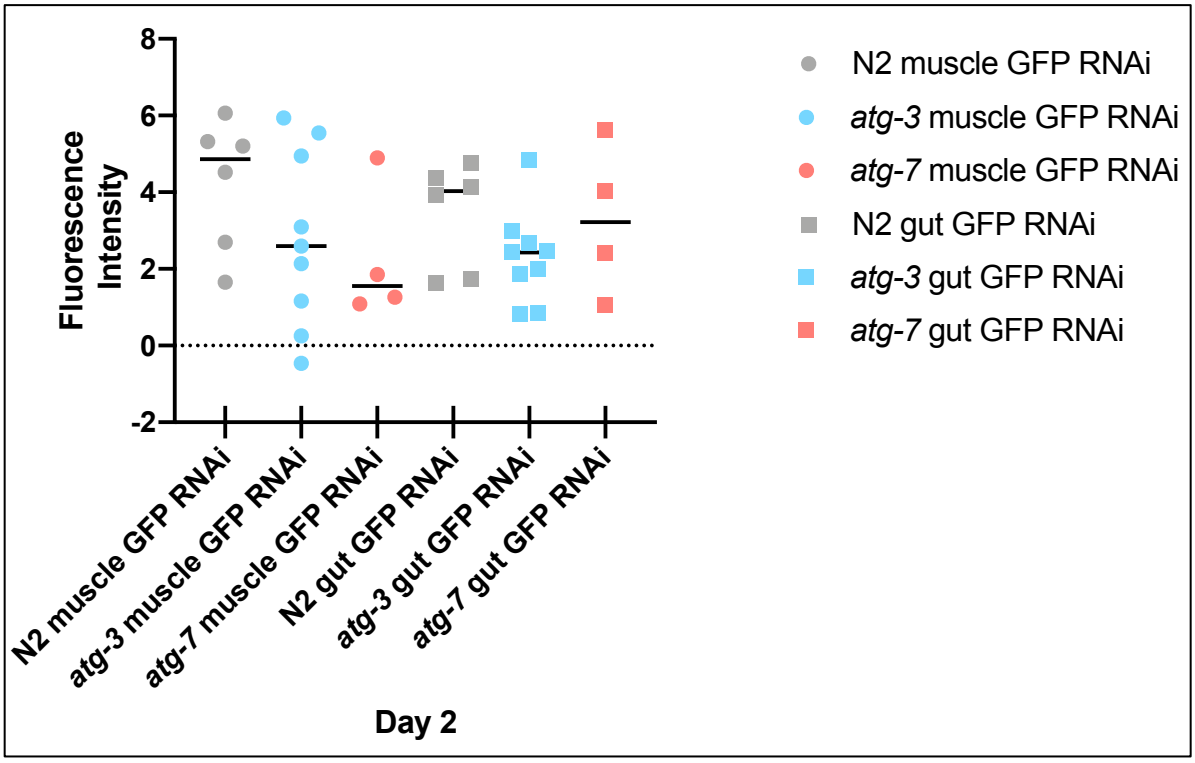

Figure 3.11
Comparison of GFP silencing between gut and muscle in three genotypes, day 2
N2 animals exposed to bacteria expressing dsRNA targeting GFP in grey. *atg-3* animals exposed to bacteria expressing dsRNA targeting GFP in light blue. *atg-7* animals exposed to bacteria expressing dsRNA targeting GFP in pink. Muscle data points are circles. Gut data points are squares. There is no detectable difference in silencing of *atg-3* and *atg-7* in muscle or gut, compared to wild type. Similarly, there is no detectable difference between muscle and gut GFP silencing in any of the three genotypes on day 2.

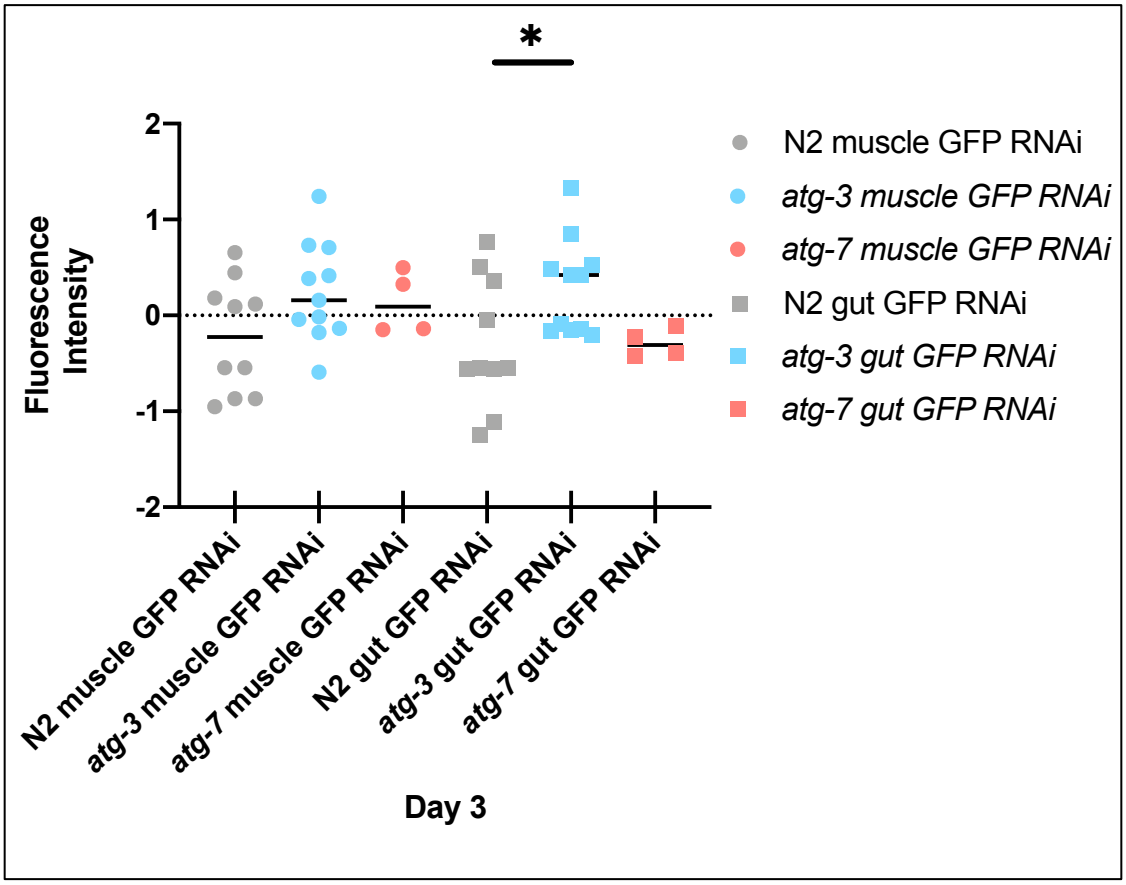

Figure 3.12
Comparison of GFP silencing between gut and muscle in three genotypes, day 3
N2 animals exposed to bacteria expressing dsRNA targeting GFP in grey. *atg-3* animals exposed to bacteria expressing dsRNA targeting GFP in light blue. *atg-7* animals exposed to bacteria expressing dsRNA targeting GFP in pink. Muscle data points are circles. Gut data points are squares. The only significant difference in GFP silencing among the autophagy mutants is the *atg-3* gut fluorescence, which is slightly higher than wild-type. There is no detectable difference between muscle and gut GFP silencing in any of the three genotypes on day 3.

Chapter 3 References

Bhatia, S., & Hunter, C. P. (2019). SID-4/NCK-1 is important for dsRNA import in Caenorhabditis elegans. bioRxiv, 702019. doi:10.1101/702019

Cadwell, K., & Debnath, J. (2017). Beyond self-eating: The control of nonautophagic functions and signaling pathways by autophagy-related proteins. Journal of Cell Biology, 217(3), 813-822. doi:10.1083/jcb.201706157

Chen, Y., Scarcelli, V., & Legouis, R. (2017). Approaches for Studying Autophagy in Caenorhabditis elegans. Cells, 6(3), 27. doi:10.3390/cells6030027

Ermolaeva, M. A., & Schumacher, B. (2014). Insights from the worm: the C. elegans model for innate immunity. Seminars in immunology, 26(4), 303-309. doi:10.1016/j.smim.2014.04.005

Feinberg, E. H., & Hunter, C. P. (2003). Transport of dsRNA into Cells by the Transmembrane Protein SID-1. Science, 301(5639), 1545-1547. doi:10.1126/science.1087117

Hinas, A., Wright, A. J., & Hunter, C. P. (2012). SID-5 is an endosome-associated protein required for efficient systemic RNAi in C. elegans. Curr Biol, 22(20), 1938-1943. doi:10.1016/j.cub.2012.08.020

Huang, S., Jia, K., Wang, Y., Zhou, Z., & Levine, B. (2013). Autophagy genes function in apoptotic cell corpse clearance during C. elegans embryonic development. Autophagy, 9(2), 138-149. doi:10.4161/auto.22352

Kaur, J., & Debnath, J. (2015). Autophagy at the crossroads of catabolism and anabolism. Nature Reviews Molecular Cell Biology, 16(8), 461-472. doi:10.1038/nrm4024

Rocheleau, Christian E. (2012). RNA Interference: Systemic RNAi SIDes with Endosomes. Current Biology, 22(20), R873-R875. doi:https://doi.org/10.1016/j.cub.2012.08.039

Shih, J. D., Fitzgerald, M. C., Sutherlin, M., & Hunter, C. P. (2009). The SID-1 double-stranded RNA transporter is not selective for dsRNA length. RNA, 15(3), 384-390. doi:10.1261/rna.1286409

Tian, Y., Li, Z., Hu, W., Ren, H., Tian, E., Zhao, Y., . . . Zhang, H. (2010). C. elegans Screen Identifies Autophagy Genes Specific to Multicellular Organisms. Cell, 141(6), 1042-1055. doi:https://doi.org/10.1016/j.cell.2010.04.034

Wang, E., & Hunter, C. P. (2017). SID-1 Functions in Multiple Roles To Support Parental RNAi in Caenorhabditis elegans. Genetics, 207(2), 547-557. doi:10.1534/genetics.117.300067

Winston, W. M., Molodowitch, C., & Hunter, C. P. (2002). Systemic RNAi in C. elegans requires the putative transmembrane protein SID-1. Science, 295(5564), 2456-2459. doi:10.1126/science.1068836

Winston, W. M., Sutherlin, M., Wright, A. J., Feinberg, E. H., & Hunter, C. P. (2007). Caenorhabditis elegans SID-2 is required for environmental RNA interference. Proceedings of the National Academy of Sciences of the United States of America, 104(25), 10565-10570. doi:10.1073/pnas.0611282104

Zhang, P., & Zhang, H. (2013). Autophagy modulates miRNA-mediated gene silencing and selectively degrades AIN-1/GW182 in C. elegans. EMBO reports, 14(6), 568-576. doi:10.1038/embor.2013.53

Chapter 4

To survive and thrive in an environment, organisms must be able to sense and respond to shifting stimuli. This is achieved in a number of ways, from sensory neurons inducing signal transduction to modulating fecundity in response to nutrient availability. Varied mechanisms contribute to this ultimate goal of survival, frequently employing the regulation of gene expression. Growing bodies of evidence indicate that species of RNA play a significant role in environmentally responsive gene regulation. In *C. elegans*, endogenously generated small RNAs (endo-siRNAs) can mediate gene expression in both a worm and its progeny (Posner et al., 2019). Systemic RNA interference (RNAi) also mediates gene expression through generations (Devanapally et al., 2015).

Foundational screens identified mutants in the spreading of systemic RNAi, termed systemic RNAi defective (SID) (W. M. Winston et al., 2002). The majority of these mutants participate in import of RNAi signals, with one, *sid-5*, involved in export. SID-5 is transmembrane protein in the late endosome, co-localizing with other late endosome proteins RAB-7 and LMP-1 (Hinas et al., 2012). The rest of the RNA export pathway, including potential points of regulation, remain unknown.

In addition to its role degrading misfolded proteins and other cell detritus, autophagy serves as an export pathway by redirecting autophagic vesicles to the cell membrane. Secretory autophagy is responsible for the export of proteins lacking a N-terminal signal sequence (e.g. yeast Acb1) and various inflammatory mediators (e.g. mammalian IL-1ß and IL-18) (Cadwell & Debnath, 2017). Recent evidence indicates that these vesicles also contain a vast number of RNA binding proteins (RBP) (Leidal et al., 2020). Here we identify an intersection between secretory autophagy and RNA export using systemic RNAi silencing as a readout.

Fluphenazine increases autophagic flux

Fluphenazine is an anti-psychotic medication that acts as an enhancer of autophagic flux (Li et al., 2014). In *C. elegans*, fluphenazine and starvation mediate increases in autophagic flux that can be visualized using strains expressing *lgg-1:mCherry,* marking autophagosomes. During a 90 minute treatment, a 10 μM concentration of fluphenazine is sufficient to increase fluorescently labeled LGG-1 autophagosomes, indicating an increase in autophagic flux (Figure 4.1) (Li et al., 2014). To assess the effect of fluphenazine alone, rather than fluphenazine coupled with starvation, worms were exposed to fluphenazine in the presence of food. Because starvation and dietary changes impact autophagic flux, a comparison between E. coli strains was necessary. OP50 is a standard bacterial strain used in the maintenance of worms, while HT115 is the bacterial strain permissive for dsRNA production. 15μM of fluphenazine paired with either OP50 or HT115 was sufficient to enhance autophagic flux, with HT115 generating a more robust response. Further, HT115 animals exposed to DMSO alone demonstrated a lower mean fluorescence intensity compared with OP50 animals exposed to DMSO, suggesting lower autophagic flux in animals fed HT115 bacteria (Figure 4.2).

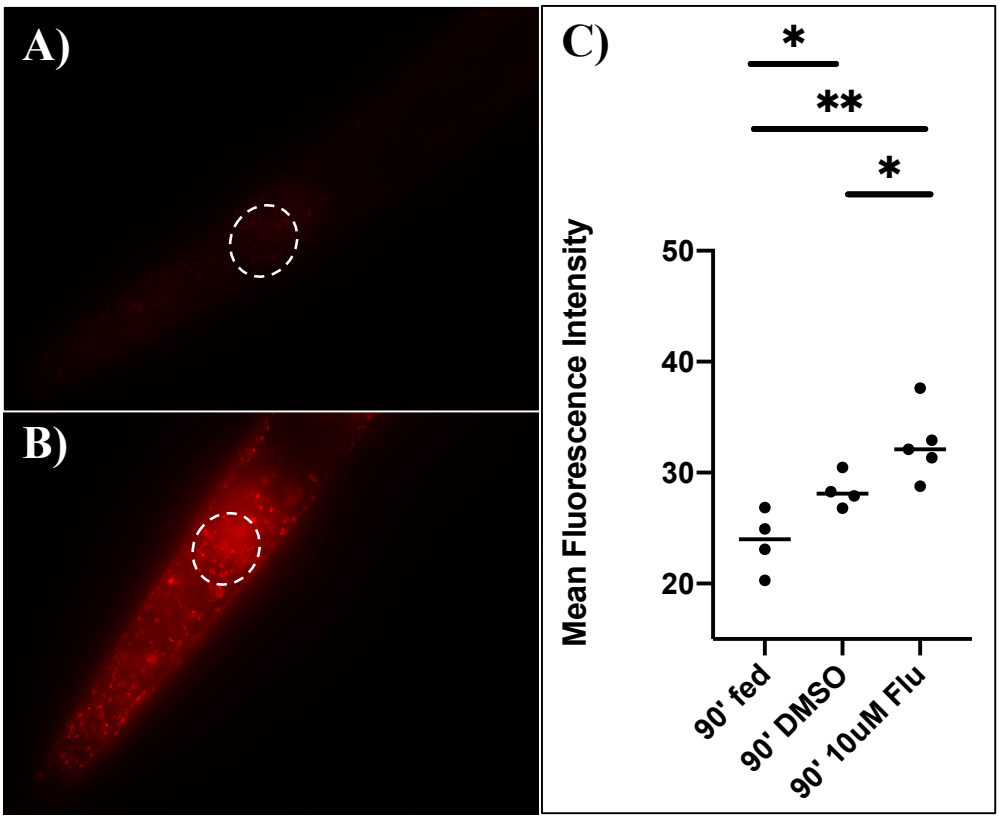

Figure 4.1
Induction and quantification of autophagy in mCherry::LGG-1 expressing strains
A) Well fed worm, grinder marked by dashed white line. B) Worm starved 6 hours, grinder marked by dashed white line. C) Mean fluorescence intensity of grinder in mCherry::LGG-1 expressing animals. Animals were rotated in liquid for 90 minutes exposed to food (OP50), 10µM DMSO or 10µM fluphenazine suspended in DMSO (Flu). Increased fluorescence was observed in animals exposed to DMSO compared to fed (unpaired t test, p=0.0282) and fluphenazine compared to fed (p=0.0036). Increased fluorescence was also observed in fluphenazine exposed animals compared to DMSO exposed animals (p= 0.0499). N=1 biological replicate.

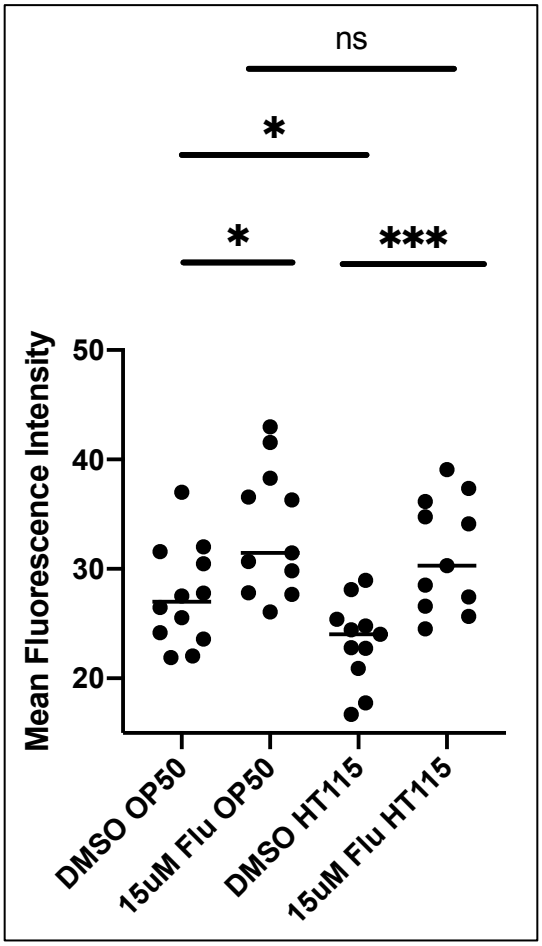

Figure 4.2
Comparison of feeding bacterial strains upon fluphenazine induction of autophagic flux
Mean fluorescence intensity of grinder region measured following a 90 minute rotation period in liquid culture containing OP50 bacteria and DMSO, OP50 bacteria and 15μM fluphenazine (in DMSO), HT115 bacteria and DMSO, or HT115 bacteria and 15μM fluphenazine (in DMSO). Exposure to fluphenazine increased mean fluorescence intensity in worms exposed to both bacterial strains (unpaired t test, OP50: p=0.0111; HT115: p=0.0005). Mean fluorescence intensity was lower in HT115 DMSO treated animals compared to OP50 DMSO treated animals (p=0.0272). The fluphenazine treated animals had similar levels of mean fluorescence intensity between the two bacterial strains (p=n.s.). N=2 biological replicates.

Fluphenazine exposure increases rate of RNAi mediated GFP silencing

To probe a possible interaction between secretory autophagy and systemic RNAi spread, worms expressing both *lgg-1:mCherry* and *myo-3:GFP* were exposed to feeding RNAi and fluphenazine. Both wild-type and *sid-5* mutants were synchronized on RNAi permissive nematode growth medium (NGM) plates seeded with HT115 bacteria expressing either an empty vector or dsRNA targeting GFP. The animals grew for 24 hours, at which point they were removed and subjected to 90 minutes of 20μM fluphenazine or DMSO exposure, in the presence of food. They were then returned to the plates. 24 hours later, the treatment was repeated, and the animals imaged under epifluorescence. The ROI for GFP was defined as the entire area anterior to the vulva. The ROI for mCherry was defined as the grinder. Both regions were defined using bright field microscopy. N2 wild-type animals exposed to DMSO and bacteria expressing dsRNA targeting GFP mostly silenced MYO-3:GFP by day 2, when compared to animals fed empty vector. N2 wild-type animals treated with 20μM fluphenazine and bacteria expressing dsRNA targeting GFP silenced completely by this time point. This effect was not observed in the sid-5 mutant background (Figure 4.3). Complete silencing was achieved in the *sid-5* mutant background by day 3, but no difference was observed between animals treated with DMSO or 20μM fluphenazine (Figure 4.4). While LGG-1:mCherry exhibited an increase in mean fluorescence intensity at day 1 (Figure 4.1-2), this increase was not seen at day 2 (Figure 4.5). This is potentially due to increased autophagic flux in older animals, masking any drug-induced increase in these animals.

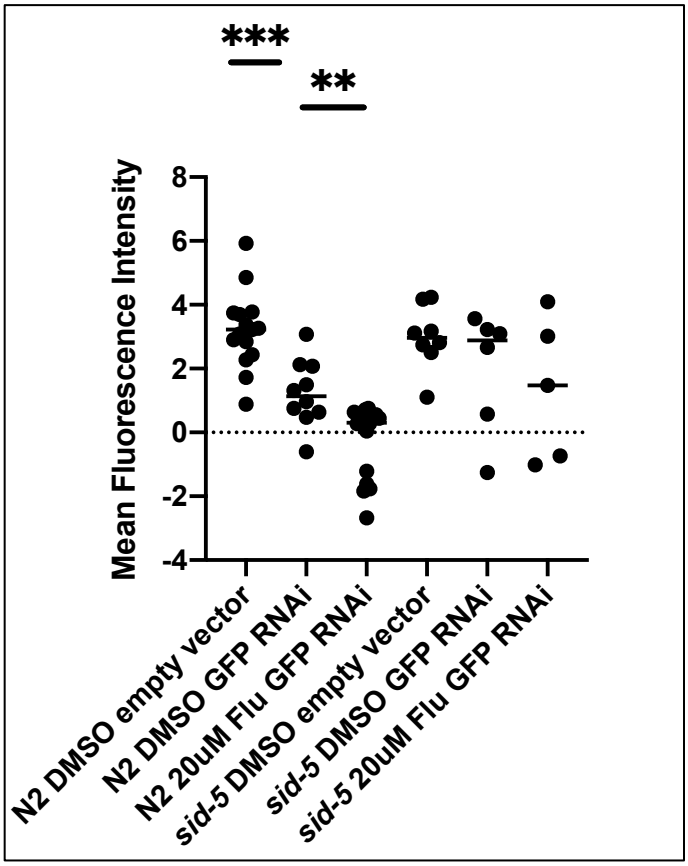

Figure 4.3
MYO-3:GFP quantification in worms undergoing systemic RNAi and fluphenazine treatment, day 2
Mean fluorescence intensity in animals on day 2 of treatment. Both negative controls, animals fed empty vector expressing bacteria, failed to exhibit GFP silencing. N2 animals exposed to DMSO and bacteria expressing dsRNA targeting GFP silenced partially compared with the empty vector control (unpaired t test, p=0.0003). N2 animals treated with 20μM fluphenazine (in DMSO) and exposed to bacteria expressing dsRNA targeting GFP silenced more compared with their DMSO treated siblings (p=0.0018). *sid-5* mutant animals all displayed the same degree of silencing, regardless of exposure to bacteria expressing empty vector or GFP targeted dsRNA, as well as DMSO or 20μM fluphenazine (in DMSO). N= 2 biological replicates, *sid-5*; N=5 biological replicates, N2.

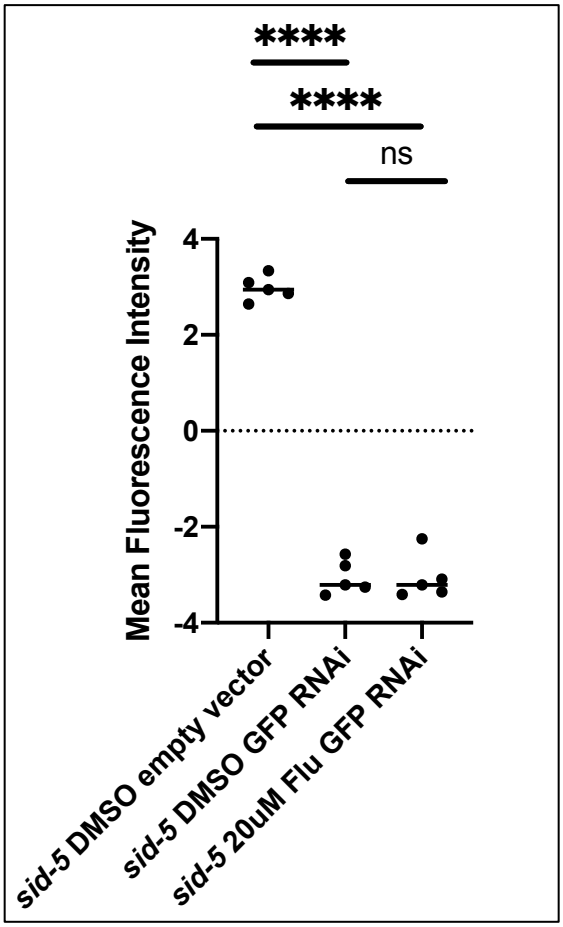

Figure 4.4
MYO-3:GFP quantification in worms undergoing systemic RNAi and fluphenazine treatment, day 3
Mean fluorescence intensity in *sid-5* mutant animals on day 3 of treatment. Worms fed bacteria expressing empty vector maintains some fluorescence. Worms fed on bacteria expressing dsRNA targeting GFP have silenced, both DMSO treated and 20µM fluphenazine (in DMSO) are significantly different from empty vector fed animals (unpaired t test, p=<0.0001, both), but demonstrate silencing similar to each other. N=1 biological replicate.

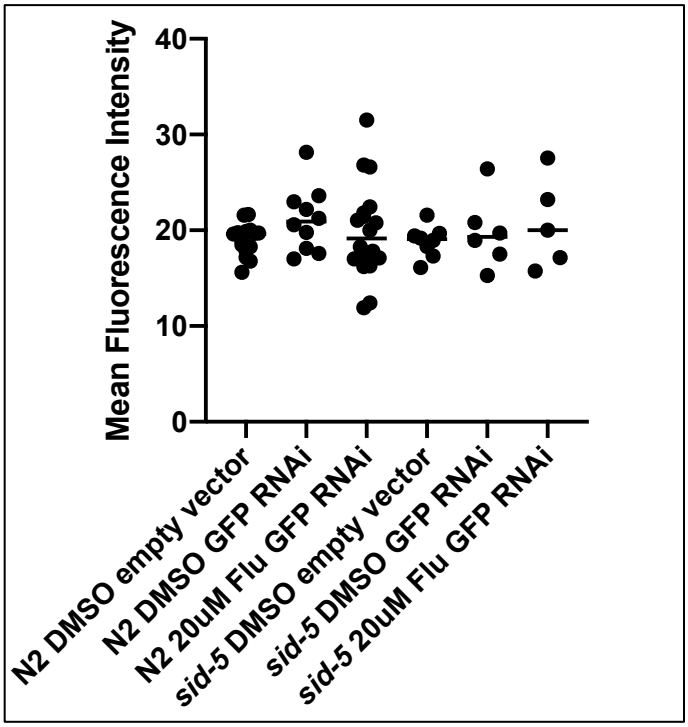

Figure 4.5
LGG-1:mCherry quantification in worms undergoing systemic RNAi and fluphenazine treatment, day 2
Mean fluorescence intensity in animals on day 2 of treatment. No variation in fluorescence was observed between the genotypes or treatment histories. N= 2 biological replicates, *sid-5*; N=5 biological replicates, N2.

To determine if repeated exposure to fluphenazine is required for the enhanced silencing effect observed in wild-type animals, cross-drug treatments were conducted. N2 wild-type animals were synchronized on plates as described earlier and subjected to DMSO or 20µM fluphenazine treatment at 24 hours. After a 24 hour recovery period, on their respective plates, animals were exposed to opposite DMSO or 20µM fluphenazine treatment. Animals exposed only once, on day 1, to 20µM fluphenazine exhibited increased silencing compared to siblings exposed to DMSO on day 1 (Figure 4.6). Further, animals exposed to fluphenazine for the first time on day 2 exhibited an increase in LGG-1:mCherry mean fluorescence intensity, suggesting that perhaps repeated exposure to the drug lessens the generation of LGG-1:mCherry

autophagosomes and possibly autophagic flux itself (Figure 4.7). These data taken together suggest that the increase in silencing seen in animals exposed to 20µM fluphenazine is dependent on the initial day 1 exposure.

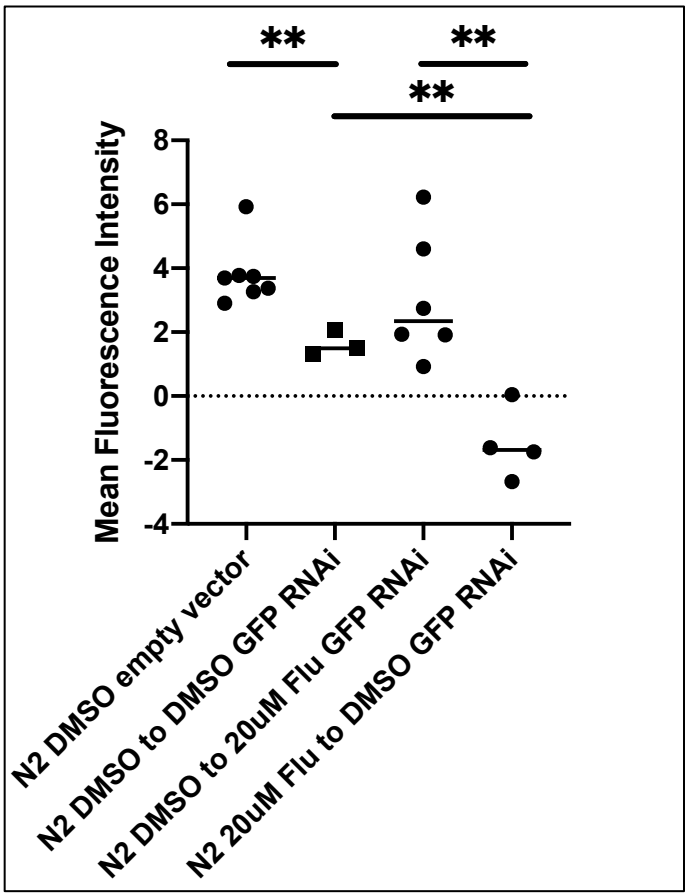

Figure 4.6
MYO-3:GFP quantification in animals cross-treated for DMSO and 20µM fluphenazine
N2 wild-type animals assessed for GFP expression on day 2. In animals only exposed to DMSO, worms fed bacteria expressing dsRNA targeting GFP partially silenced when compared to worms fed empty vector control (unpaired t test, p=0.0067). Worms exposed DMSO on day 1 and 20µM fluphenazine on day 2 exhibited the same degree of silencing as siblings treated with DMSO only. Worms exposed to 20µM fluphenazine on day 1 and DMSO on day 2 exhibited increased silencing on day 2, when compared to worms exposed to DMSO on day 1 (p=0.0065 and p=0.0033, respectively). N= 2 biological replicates.

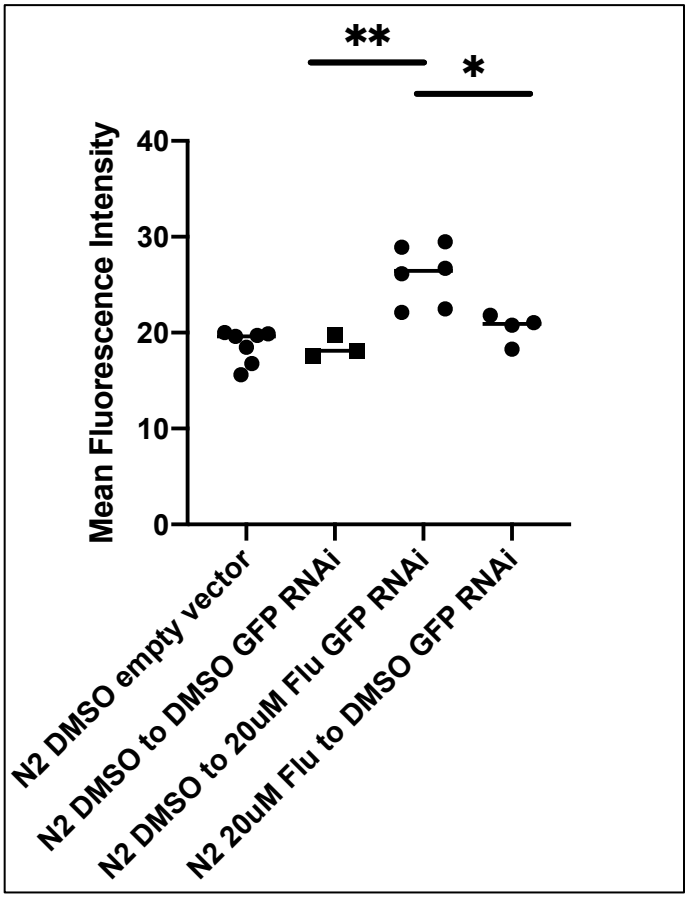

Figure 4.7
LGG-1:mCherry quantification in animals cross-treated for DMSO and 20µM fluphenazine. N2 wild-type animals assessed for mCherry expression on day 2. All animals exposed to DMSO on day 2 exhibited similar mean fluorescence intensity. Animals exposed to 20µM fluphenazine for the first time on day 2 exhibited an increase in mean fluorescence intensity compared to DMSO treated siblings ($p=0.0058$ and $p=0.0122$, respectively). N= 2 biological replicates.

Transient starvation does not increase rate of RNAi mediated GFP silencing

Starvation is another key activator of autophagic flux. To determine if starvation contributes to an increased rate of systemic RNAi silencing, wild-type worms expressing lgg-1:mCherrry and myo-3:GFP were raised on HT115 bacteria expressing empty vector or dsRNA. These animals were periodically starved and monitored for GFP silencing. Worms starved for different periods of time in liquid or on solid media reflected different mean fluorescence intensity of LGG-1:mCherry, a proxy for increased autophagic flux. Starvation in liquid failed to induce any changes in intensity, possible due to overall exertion from swimming. Starvation on plates induced an increase in intensity at 6 hours only (Figure 4.8)

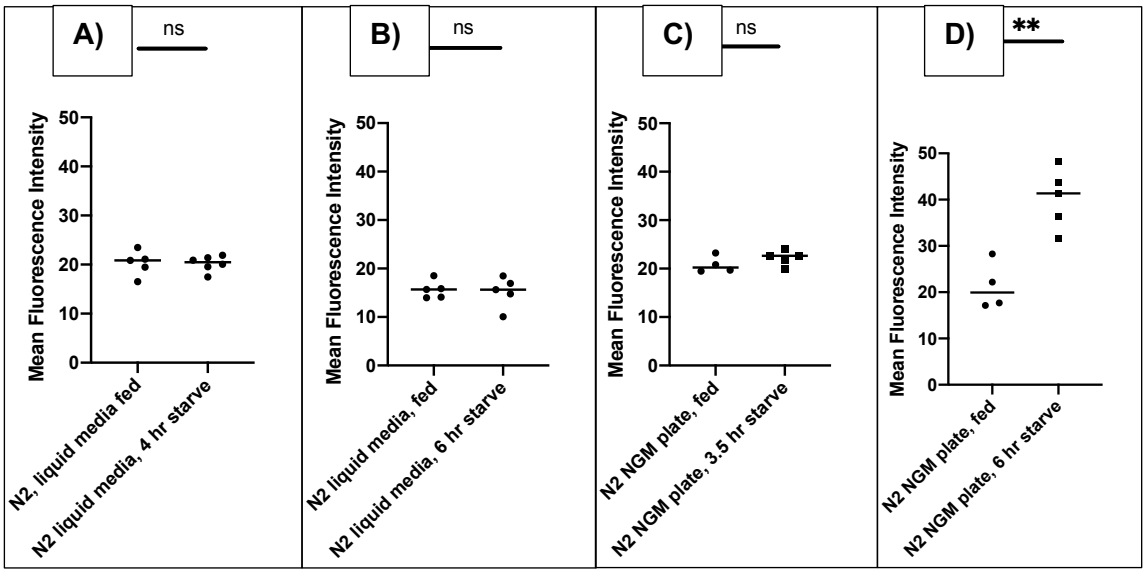

Figure 4.8
Quantification of LGG-1:mCherry in animals under differing starvation treatments
A) 4 hours of starvation in liquid culture was not sufficient to induce measurable increases in mean fluorescence intensity. B) 6 hours of starvation in liquid culture was not sufficient to induce measurable increases in mean fluorescence intensity. C) 3.5 hours of starvation on NGM plates was not sufficient to induce measurable increases in mean fluorescence intensity. D) 6 hours of starvation on NGM plates induced an increase in mean fluorescence intensity ($p=0.0021$). N= 1 biological replicate.

sid-5 mutant and N2 wild-type animals were synchronized onto RNAi permissive plates seeded with bacteria expressing either empty vector or dsRNA targeting GFP and allowed to grow. At 24 hours, a cohort was removed and starved on unseeded NGM plates for 6 hours, after which they were returned to appropriate RNAi plates. 24 hours following this treatment they were mounted and imaged using an epifluorescence scope to quantify GFP expression. Neither *sid-5* mutants nor N2 wild-type animals demonstrated any change in GFP silencing compared to control.

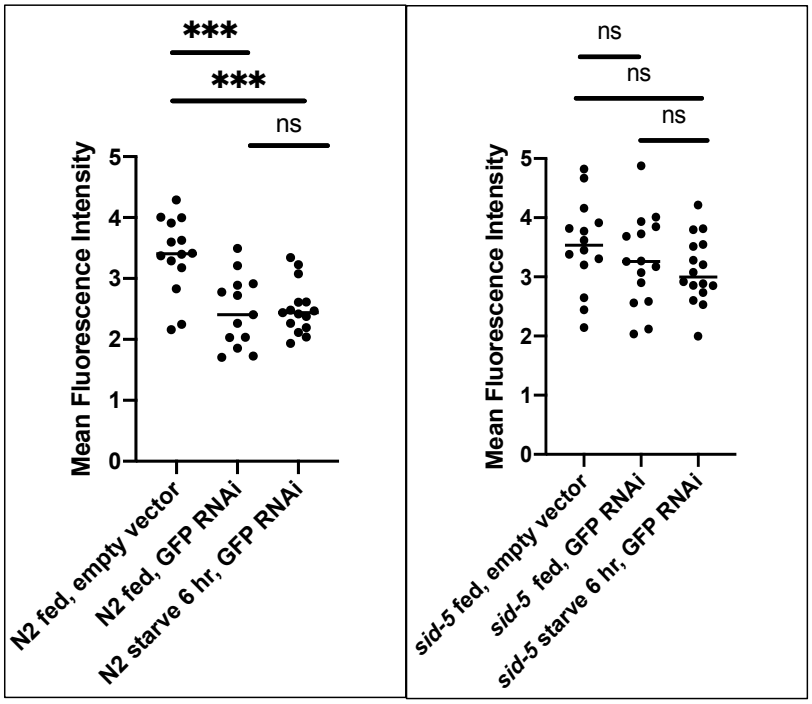

Figure 4.9
MYO-3:GFP quantification in fed and starved animals
Quantification of GFP expression on day 2 of *sid-5* and N2 wild-type animals raised on RNAi plates. A) N2 animals silenced when fed bacteria expressing dsRNA targeting GFP, with a 6 hour starvation period having no impact on silencing. B) *sid-5* animals failed to silence by day 2 under any treatment. N=3 biological replicates.

While fluphenazine and starvation are both enhancers of autophagic flux, only fluphenazine is successful in increasing systemic RNAi silencing. It is possible that this drug's specificity permits an increase in secretory autophagy without incurring off-target effects. Starvation initiates an array of biological responses, some of which may confound systemic RNAi export. It is also important to consider feeding behavior directly following a period of starvation. Increased consumption of bacteria expressing dsRNA targeting GFP may alter the silencing landscape within a worm.

sid-5 mutants demonstrate increased LGG-1:mCherry fluorescence intensity following fluphenazine treatment (not shown), but do not show decreased MYO-3:GFP fluorescence intensity. This is consistent with SID-5 acting as a late endosomal protein. SID-5 likely impairs later stages of secretory autophagy.

The ability of fluphenazine to increase the rate of systemic RNAi silencing opens up new experimental avenues of RNA export regulation. Further validation of this system requires analysis of tissue specific RNAi mediated silencing in order to verify its role in the spread of systemic silencing, as opposed to the efficiency of cell autonomous silencing. In this vein, RNA fluorescent in situ hybridization (FISH) against dsRNA GFP would illuminate the distribution of the silencing signal. This would reveal how fluphenazine impacts the localization of biologically active RNA species.

The ability of fluphenazine to act in such a targeted manner suggests that other drugs may be able to impact the regulation of secretory autophagy mediated RNA export. Of primary importance is bafilomycin-A, a drug that blocks the acidification of autophagosomes. In model organisms, this leads to a build-up of autophagosomes in affected tissues. Whether this build-up

of autophagosomes blocks all autophagy or redirects autophagosomes to a secretory autophagy fate is unknown. But either fate would be useful in experimental settings.

If drugs are capable of mediating the rate of RNA export via the secretory autophagy pathway, one must consider if this phenomenon occurs outside the lab. A close exploration of physiological states and environmental elements may reveal an *in vivo* mediator of RNA export. Whether a pathogen or environmental contaminant or something more benign, a "naturally occurring" RNA export mediator could drastically impact our views on how RNA acts in an organism. Regulating the export of biologically active RNA species presents another layer of gene regulation.

The intersection between secretory autophagy and systemic RNAi illuminates a new perspective on RNA export. Autophagy is a process that can be influenced by both environmental stimuli as well as artificial means, thus providing a point of regulation for RNA export. Framing RNA mediated silencing as a regulatable process broadens the understanding of environmentally responsive RNAs as well as serving as a useful tool in a laboratory setting.

Chapter 4 References

Cadwell, K., & Debnath, J. (2017). Beyond self-eating: The control of nonautophagic functions and signaling pathways by autophagy-related proteins. Journal of Cell Biology, 217(3), 813-822. doi:10.1083/jcb.201706157

Devanapally, S., Ravikumar, S., & Jose, A. M. (2015). Double-stranded RNA made in C. elegans neurons can enter the germline and cause transgenerational gene silencing. Proc Natl Acad Sci U S A, 112(7), 2133-2138. doi:10.1073/pnas.1423333112

Hinas, A., Wright, A. J., & Hunter, C. P. (2012). SID-5 is an endosome-associated protein required for efficient systemic RNAi in C. elegans. Curr Biol, 22(20), 1938-1943. doi:10.1016/j.cub.2012.08.020

Leidal, A. M., Huang, H. H., Marsh, T., Solvik, T., Zhang, D., Ye, J., . . . Debnath, J. (2020). The LC3-conjugation machinery specifies the loading of RNA-binding proteins into extracellular vesicles. Nature Cell Biology, 22(2), 187-199. doi:10.1038/s41556-019-0450-y

Li, J., Pak, S. C., O'Reilly, L. P., Benson, J. A., Wang, Y., Hidvegi, T., . . . Perlmutter, D. H. (2014). Fluphenazine reduces proteotoxicity in C. elegans and mammalian models of alpha-1-antitrypsin deficiency. PloS one, 9(1), e87260. doi:10.1371/journal.pone.0087260

Posner, R., Toker, I. A., Antonova, O., Star, E., Anava, S., Azmon, E., . . . Rechavi, O. (2019). Neuronal Small RNAs Control Behavior Transgenerationally. Cell, 177(7), 1814-1826.e1815. doi:https://doi.org/10.1016/j.cell.2019.04.029

Winston, W. M., Molodowitch, C., & Hunter, C. P. (2002). Systemic RNAi in C. elegans requires the putative transmembrane protein SID-1. Science, 295(5564), 2456-2459. doi:10.1126/science.1068836

Experimental procedures

Strains and maintenance

Bristol N2, jz2171 (*pmyo-3:GFP; lgg-1:mCherry; sid-5(ok3517)*), jz2175 (*pmyo-3:GFP; lgg-1:mCherry*), jz2169 (*pelt-2:GFP; pmyo-3:GFP*), jz2170 (*pmyo-3:GFP; sid-5(ok3517)*), jz2176 (*pelt-2:GFP; pmyo-3:GFP; atg-3 (bp412)*), jz2177 (*pelt-2:GFP; pmyo-3:GFP* ; *sid-5(ok3517)*), jz2179 (*pmyo-3:GFP; atg-7(bp411)*), cx5922 (*kyIs140 [str-2::GFP + lin-15(+)] I; ceh-36* (ky640) X), jz1524 (*sid-1(pk3321)*), HZ1684 (*atg-3(bp412); him-5(e1490)*), HZ1686 (*atg-7(bp411); him-5(31490)*), jz894 *(mut-7(pk204*)), XWS-967 (*lgg-1:mCherry:*LGG-1*),* were used in this study. Strains were maintained under standard protocols (Brenner, 1974).

Chemotaxis and adaptation training

Chemotaxis was performed as described in (C. I. Bargmann et al., 1993). Butanone adaptation assays were performed as described in (L'Etoile et al., 2002), with butanone training buffer at 11µl butanone: 100ml S. basal. A small cohort of worms were removed from each condition to assess behavior, while the rest were frozen in liquid nitrogen and stored at -80ºC for RNA extraction.

Small RNA sequencing libraries

4 biological replicates of N2 and 3 biological replicates of sid-1 (pk3321) underwent butanone adaptation training and were frozen at -80. RNA was harvested using Qiagen miRNAeasy Micro Kit (Qiagen cat# 217084). Following DNAse treatment (Turbo DNAse treatment, ThermoFisher cat# AM2239), samples were run on a 1% EtBr gel to confirm quality

and size of RNA. Samples were then submitted for RNA sequencing and bioinformatical analysis to the UCSF Genome Center.

22G RNA quantification

22G RNA quantification was achieved with custom ThermoFisher TaqMan probes, described in tables 1.1 and 1.3. RNA was extracted as above, using Qiagen miRNAeasy kits and Turbo DNAse. Reverse transcription was completed using ABI Multiscribe Reverse Trasncriptase (now ThermoFisher cat# 4311235). Analysis was carried out both BioRad and QuantStudio 6 machines.

mRNA quantification

mRNA quantification was extracted from frozen worm pellets. In starvation assays, worms were in liquid culture, either diluted OP50 or S. basal, for 60 minutes before freezing. In S. marcescens infection assays, L4 worms were place on plates containing equally sized lawns of OP50 and S. marcescens, and left for 24 hours before freezing. mRNA was extracted using RNeasy Mini Kit (Qiagen cat# 74104) and Turbo DNAse. cDNA synthesis was accomplished using SuperScriptIII Reverse Transcriptase (ThermoFisher cat# 18080044). Primer sequences listed on table S.1 and were quantified with SYBR Green (ThermoFisher cat# 4309155) on a QuantStudio 6 qPCR machine.

Table S.1
Primers used for mRNA quantification

name	forward primer	reverse primer
odr-1	GCGAAGACCCCTACCATTTA	CGCTGGCAACATTTCATTTA
unc-40	GGTGGAATAGGTGGTCTTGG	CATTGGGAGAGGCGGAGT
mks-5 (primer set 2)	GCTCGTGCATCAATCCCTATC	GCCGTTTTCGAATTGGCTCA
sol-2 (primer set 2)	CGTCAGAGACGTCTGAAGCA	CGCAAATTCCATGACCCTGT
egl-21 (primer set 1)	AAGTGCCCAGAGATCACCAC	CCAAGAGCAAGCTCGAAACC
daf-7 (primer set 1)	CCCTTCATCCCCAACAGACC	CCAAGTTGAAGTGGTGTGCG
daf-7 (primer set 5)	GATGAAGCAGCACCGAACAG	CTGTGAGTGTGGCCTGAAGAA
mapk-15 (primer set 4)	CGACGAACACCCGTAAACAT	GTATCACCATCGGAGCGTCG
Y11 (primer set 2)	CAGGCGGCTCAAGTGTTTTT	CGAGTCGATGTGCAGTCTATCA
trp-4 (primer set 2)	TTGCCGCAAAATTCGGTCAG	GGCTAGGGAACCCTTCATCG
arl-13 (primer set 1)	ATGTTTTGGCATCGGAAGCG	AGGGAGTGGAGAGCCTCAAT
dyf-3 (primer set 3)	AGCTGAGAAACCTGTGTGAGA	AGCTGAGAAACCTGTGTGAGA
mod-5 (primer set 1)	TGCCCGTTGTTTCGAGGAAT	TGACGGAGTGGTCAATGGTG
mod-5 (primer set 2)	TTTGGAAGGGTCCACAGTCG	CGGCGTCACGATAGCAGTTA

Table S.1 (continued)

name	forward primer	reverse primer
capa-1 (primer set 1)	AATGATTTCTCCTTGCAACGAATTG	AACACGCGCCATGTAGAGTC
unc-10 (primer set 4)	AGGGGAGCAGAAGGGAAAAG	TTGACGACCGACAACCTGAC

QUAS-Dexamethasone plasmid and strain construction

To generate the first neuronally expressed QF-Dex(LBD) construct, I excised the H20 promoter from H20p in pPD95.75 (gift from M. Gallegos), using restriction enzyme digestion (SphI and AscI). I then inserted this fragment into SphI/AscI digested pGM32, to generate the finished construct. To generate the 5XQUAS hpGFP construct, I digested out the hairpin sequence (including unc-22 loop) with AgeI and AflII from pHC377 (gift from A. Jose). I also digested pGM34 with AscI and SpeI. I blunted the products of these two reactions and then ligated them together. Using sequencing verification, I was able to confirm both constructs (pKM11 and pKM12, respectively). I also modified pXW82 from (Wei et al., 2012), to express GFP both in forward and reverse orientation. pGM32, pGM34 and XW82 were gifts from G. Monsalve, but are also available on Addgene.

pKM11 and pKM12 were injected at 40ng/µl each into sur-5:GFP expressing worms to generate dexamethasone inducible worms. pKM11, pKM20 and pKM21 were injected at ratios of 40ng/µl: 20ng/µl: 20ng/µl as well as 40ng/µl: 10ng/µl: 30ng/µl in an effort to generate an inducible silencing strain. All injections were accompyaned with pmyo-3:dsRed as a co-injection marker at 5ng/µl.

All dexamethasone treatments were carried out as described in (Monsalve et al., 2019), with KRY569 serving as a positive control. Worms were monitored on fluorescent dissecting scope as well as an inverted epiflorescent scope for silencing.

mRNA probes of Dexamethasone inducible strains

Strains carrying the pH20:QF-GR(LBD) construct and purportedly carrying the 5XQUAS:hpGFP construct were sorted into transgenic positive and transgenic negative animals. Both of these pools were subjected to dexamethasone induction for 4 hours. After which, animals were frozen in liquid nitrogen and stored at -80ºC. mRNA was extracted as previously described. Primer sequences listed in table S.2.

Table S.2
Primers used to probe expression of hpGFP
Amplifies region at the junction between GFP and unc-22 loop.

	Forward sequence	Reverse sequence
Primer set 1	ACC TGT CCA CAC AAT CTG CC	TTG ACA GCC TTG ACA CGG AA
Primer set 2	GCG ATG GCC CTG TCC TTT TA	CAG CCT TGA CAC GGA ACT GA
Primer set 3	CCA CAC AAT CTG CCC TTT CG	TGA CAG CCT TGA CAC GGA AC
Primer set 4	AAG CGA AGA CTA CAA GAC CCG	CTG TCC ACA CAA TCT GCC CTT

Table S.2 (continued)

	Forward sequence	Reverse sequence
Primer set 5	AGA CCC GAT TTG TGC TCC G	TGG GAT TAC ACA TGG CAT GGA
Primer set 6	TCG ATG TTC CAG TAC GCG G	CTG CTG GGA TTA CAC ATG GCA

Cell corpse counting

Young adult N2 wild-type, *atg-3* (bp412) and *atg-7* (bp411) mutants were allowed to roam a seeded NGM plate for 2 hours and then removed. 4-6 hours later, embryos were mounted onto slides and imaged on a Zeiss Axiovert 200M, using differential interference contrast (DIC) microscopy. Embryos at bean stage (6 hpf) were captured as z-stacks covering the entire embryo. Stacks were then blinded and counted for cell corpses.

Qualification of GFP expression in wild-type, autophagy and *sid-5* mutants

Young adult animals, both wild-type and mutants, expressing *myo-3:GFP(NLS)* were placed on 60mm RNAi permissive plate (Teknova cat# N0197) and allowed to roam for 1-2 hours, after which they were removed and burned. Plates were seeded with 500 ml of HT115 bacteria expressing both empty vector and dsRNA targeting GFP. Bacteria was cultured overnight from one colony in 100ml LB. Developing embryos at this point are designated Day 0. On Days 2 and 3, the worms, remaining on their plates, were examined on a fluorescent dissecting scope, with each animal scored 1-4: 1) GFP expressing fully 2) GFP mostly on 3) GFP mostly off 4) GFP completely silenced. These categories reflect the number of muscle nuclei expressing GFP, and how brightly. This was repeated 5 times with 30-60 animals per plate.

Quantification of GFP expression in wild-type and autophagy mutants

Young adult animals, both wild-type and mutants, expressing *myo-3:GFP(NLS)* and *elt-2:GFP(NLS)* were placed on 60mm RNAi permissive plate (Teknova cat# N0197) and allowed to roam for 2-3 hours, after which they were removed and burned. Plates were seeded with 500 ml of HT115 bacteria expressing both empty vector and dsRNA targeting GFP. Bacteria was cultured overnight from one colony in 100ml LB. Developing embryos at this point are designated Day 0. On days 2 and 3, animals have reached the L4 and adult stage respectively, and a portion are removed for imaging. Animals of all three genotypes, and fed both types of HT115, were mounted using the paralytic sodium azide and imaged on a Zeiss Axiovert 200M using epifluorescence. Z plane images of the entire animal were obtained in both red and green channels, as well as a brightfield reference image using a 20X objective. Each channel was stacked with the brightfield reference using Fiji. Using the brightfield reference, a ROI was defined as the anterior half of the worm, using the developing vulva as a marker. The ROI was divided into two distinct anatomical regions, intestine and muscle. Muscle was defined as anything not intestine, which was sufficient as GFP was expressed under intestinal and muscle specific promoters. Using Fiji, the overall area was measured. The mean fluorescence intensity of each plane was measured in each tissue type, as well as 3 points of background outside of the worm. These intensities were averaged among planes, then background intensity was subtracted from muscle and intestine. These values are plotted. This was repeated 2-5 times, with 2-4 animals analyzed per condition.

Fluphenazine treatments

Both wild-type and sid-5 mutant animals expressing *myo-3:GFP* and *lgg-1:mCherry* were exposed to these drug treatments. To synchronize animals, one 100mm confluent plate of worms was bleached and then distributed to 8 60mm RNAi plates, half seeded with empty vector HT115 and half seeded with HT115 expressing dsRNA targeting GFP. 24 hours later at 20ºC, animals were rinsed using S. basal into a 1.5ml eppendorf tube, allowed to settle and then liquid removed from the pellet. The pellet was then suspended in 980µl of cognate dilute bacteria. 0.255mg of powdered fluphenazine was suspended in 500ml of DMSO (Sigma cat# F4765) to a concentration of 1M. For most experiments, either 20µl of this stock solution or 20µl of DMSO was added to the worm/bacteria and rotated for 90 minutes. For pilot experiments, concentrations of 10µl and 15µl were used as well as HT115 bacteria and OP50. All experiments were conducted with a total volume of 1ml. After this time period, the animals were rinsed 3 times in S. basal and returned to new cognate RNAi plates. They were either immediately imaged or left to recover one day before repeated treatment, and then imaged.

Imaging fluphenazine treated animals

Immediately following drug or control treatment, worms were paralyzed with sodium azide and imaged on a Zeiss Axiovert 200M microscope under bright field and epifluorescence. A z-stack was taken in both the red and green channels as well as a bright field reference using a 20X objective. These images were compiled into either red or green stacks, with a bright field reference, using Fiji. For images of MYO-3:GFP, the ROI was defined as the anterior half of the worm, using the developing vulva as reference. Three areas outside the worm were selected for background. For images if LGG-1:mCherry, the ROI was defined by the grinder. For GFP, the

mean fluorescence intensity was measured for each plane, and then averaged together. The three background areas were averaged and then subtracted from the ROI intensity. For mCherry, the mean fluorescence intensity was measured for each plane. Extremely low values (- 5% of the total mean) were excluded, as the entire stack included images that were in focus for GFP expression but out of focus for the grinder. All values were plotted.

Starvation treatments

All animals were synchronized as they were for fluphenazine treatments, above. For pilot experiments, synchronized L4 animals were rinsed and suspended in S basal or dilute OP50 for 4-6 hours. Synchronized L4 animals were also rinsed and plated on unseeded 100mm NGM plates for 3.5-6 hours. After this period of starvation, animals were paralyzed with sodium azide and imaged on a Zeiss Axiovert 200M as described above. Only mCherry was measured (to assess autophagic flux).

To assess potential changes in GFP silencing, animals were synchronized onto RNAi plates as above. After 24 hours, animals were starved for 6 hours on NGM plates. After this period, animals were returned to new cognate RNAi plates. After recovering for 24 hours, they were removed from their RNAi plates, mounted and paralyzed and imaged as above.

Experimental Procedures References

Bargmann, C. I., Hartwieg, E., & Horvitz, H. R. (1993). Odorant-selective genes and neurons mediate olfaction in C. elegans. Cell, 74(3), 515-527. doi:10.1016/0092-8674(93)80053-h

Brenner, S. (1974). The genetics of Caenorhabditis elegans. Genetics, 77(1), 71-94. 2

Juang, B.-T., Gu, C., Starnes, L., Palladino, F., Goga, A., Kennedy, S., & L'Etoile, Noelle D. (2013). Endogenous Nuclear RNAi Mediates Behavioral Adaptation to Odor. Cell, 154(5), 1010-1022. doi:https://doi.org/10.1016/j.cell.2013.08.006

L'Etoile, N. D., Coburn, C. M., Eastham, J., Kistler, A., Gallegos, G., & Bargmann, C. I. (2002). The Cyclic GMP-Dependent Protein Kinase EGL-4 Regulates Olfactory Adaptation in C. elegans. Neuron, 36(6), 1079-1089. doi:https://doi.org/10.1016/S0896-6273(02)01066-8

Monsalve, G. C., Yamamoto, K. R., & Ward, J. D. (2019). A New Tool for Inducible Gene Expression in <em>Caenorhabditis elegans</em&gt. Genetics, 211(2), 419. doi:10.1534/genetics.118.301705

Wei, X., Potter, C. J., Luo, L., & Shen, K. (2012). Controlling gene expression with the Q repressible binary expression system in Caenorhabditis elegans. Nature Methods, 9(4), 391-395. doi:10.1038/nmeth.1929

Publishing Agreement

It is the policy of the University to encourage open access and broad distribution of all theses, dissertations, and manuscripts. The Graduate Division will facilitate the distribution of UCSF theses, dissertations, and manuscripts to the UCSF Library for open access and distribution. UCSF will make such theses, dissertations, and manuscripts accessible to the public and will take reasonable steps to preserve these works in perpetuity.

I hereby grant the non-exclusive, perpetual right to The Regents of the University of California to reproduce, publicly display, distribute, preserve, and publish copies of my thesis, dissertation, or manuscript in any form or media, now existing or later derived, including access online for teaching, research, and public service purposes.

DocuSigned by:
Katharine Mellman
CA5F321C846A4FF...
Author Signature

3/18/2020
Date